Article

Developmental Cell

A Hippo-like Signaling Pathway Controls Tracheal Morphogenesis in *Drosophila melanogaster*

Graphical Abstract

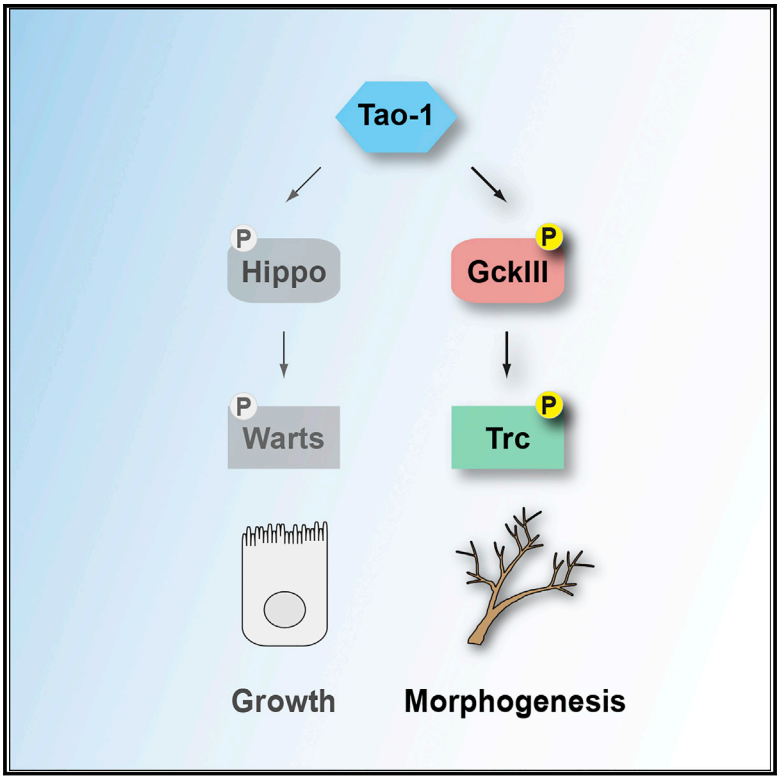

Highlights

- The Tao-1 kinase regulates GckIII kinase activity in both flies and humans
- Tao-1, GckIII, and Tricornered kinases constitute a Hippo-like signaling pathway
- This Hippo-like pathway regulates tube architecture in the fly tracheal system

Authors

Carole L.C. Poon, Weijie Liu, Yanjun Song, ..., Alexander Hergovich, Amin Ghabrial, Kieran F. Harvey

Correspondence

kieran.harvey@petermac.org

In Brief

Poon et al. describe the discovery of a Hippo-like signaling pathway comprising the kinases Tao-1, GckIII, and Tricornered and its role in tracheal morphogenesis in *Drosophila*. These discoveries enhance our understanding of tube formation and have the potential to offer insights into the human vascular disease cerebral cavernous malformation.

Poon et al., 2018, Developmental Cell *47*, 1–12
December 3, 2018
https://doi.org/10.1016/j.devcel.2018.09.024

CellPress

Please cite this article in press as: Poon et al., A Hippo-like Signaling Pathway Controls Tracheal Morphogenesis in *Drosophila melanogaster*, Developmental Cell (2018), https://doi.org/10.1016/j.devcel.2018.09.024

Developmental Cell
Article

A Hippo-like Signaling Pathway Controls Tracheal Morphogenesis in *Drosophila melanogaster*

Carole L.C. Poon,[1,2] Weijie Liu,[3] Yanjun Song,[3] Marta Gomez,[4] Yavuz Kulaberoglu,[4] Xiaomeng Zhang,[1,2] Wenjian Xu,[5] Alexey Veraksa,[5] Alexander Hergovich,[4] Amin Ghabrial,[3,8,9] and Kieran F. Harvey[1,2,6,7,8,9,10,*]
[1]Peter MacCallum Cancer Centre, 305 Grattan St, Melbourne, VIC 3000, Australia
[2]Sir Peter MacCallum Department of Oncology, University of Melbourne, Parkville, VIC 3010, Australia
[3]Department of Pathology and Cell Biology, Columbia University College of Physicians and Surgeons, 630 West 168th Street, New York, NY 10032, USA
[4]University College London, Cancer Institute, London WC1E 6BT, UK
[5]Department of Biology, University of Massachusetts Boston, Boston, MA 02125, USA
[6]Department of Pathology, University of Melbourne, Parkville, VIC 3010, Australia
[7]Department of Anatomy and Developmental Biology and Biomedicine Discovery Institute, Monash University, Clayton, VIC 3168, Australia
[8]These authors contributed equally
[9]Senior author
[10]Lead Contact
*Correspondence: kieran.harvey@petermac.org
https://doi.org/10.1016/j.devcel.2018.09.024

SUMMARY

Hippo-like pathways are ancient signaling modules first identified in yeasts. The best-defined metazoan module forms the core of the Hippo pathway, which regulates organ size and cell fate. Hippo-like kinase modules consist of a Sterile 20-like kinase, an NDR kinase, and non-catalytic protein scaffolds. In the Hippo pathway, the upstream kinase Hippo can be activated by another kinase, Tao-1. Here, we delineate a related Hippo-like signaling module that Tao-1 regulates to control tracheal morphogenesis in *Drosophila melanogaster*. Tao-1 activates the Sterile 20-like kinase GckIII by phosphorylating its activation loop, a mode of regulation that is conserved in humans. Tao-1 and GckIII act upstream of the NDR kinase Tricornered to ensure proper tube formation in trachea. Our study reveals that Tao-1 activates two related kinase modules to control both growth and morphogenesis. The Hippo-like signaling pathway we have delineated has a potential role in the human vascular disease cerebral cavernous malformation.

INTRODUCTION

Signaling pathways that contain a Sterile 20-like kinase that activates a nuclear Dbf2-related (NDR) family kinase exist throughout eukaryotes, regulate different biological processes, and are sometimes referred to as Hippo-like signaling modules (Hergovich and Hemmings, 2012). Antecedent examples of this type of kinase module include the *Saccharomyces cerevisiae* mitotic exit network and the *Schizosaccharomyces pombe* septation initiation network, which control cell division and cytokinesis (Bardin and Amon, 2001). The best-defined signaling module of this kind in metazoans forms the core of the Hippo pathway, which operates in insects and mammals to control processes such as organ size and cell fate (Pan, 2010; Halder and Johnson, 2011; Harvey et al., 2013). In addition, a related pathway has been identified in mammals and consists of the Sterile 20-like kinase Mammalian Sterile Twenty-like 3 (MST3) (and possibly its close homologs MST4 and STK25), which can regulate the NDR family kinases NDR1 and NDR2 (aka STK38 and STK38L) (Hergovich, 2013). In some instances, Sterile 20-like kinases have been reported to regulate more than one type of NDR family kinase. For example, Hippo (Hpo) can regulate both Tricornered (Trc) and Warts (Wts) in *Drosophila melanogaster* peripheral nervous system dendrites (Emoto et al., 2006). In addition, in mammals, the Hpo orthologs MST1 and MST2 can regulate both the Trc orthologs NDR1 and NDR2 and the Wts orthologs LATS1 and LATS2 (Yu and Guan, 2013; Hergovich and Hemmings, 2009; Avruch et al., 2012).

The sole *D. melanogaster* ortholog of NDR1/2, Trc, controls hair and bristle development in the wing, thorax, and antennae, as well as dendrite tiling and branching in the peripheral nervous system (Geng et al., 2000; Emoto et al., 2006). In *D. melanogaster*, the sole ortholog of MST3/MST4/STK25, Germinal center kinase III (GckIII), regulates tracheal development together with the non-catalytic protein Cerebral cavernous malformation 3 (CCM3). Loss of *GckIII* results in a characteristic dilation at the transition zone of the terminal cell, associated with abnormal localization and abundance of septate junction proteins and the apical membrane protein Crumbs (Song et al., 2013). The mechanism by which GckIII is regulated in trachea is unknown, and it is also unclear whether GckIII controls tracheal development by regulating an NDR family kinase.

Kinases belonging to the Thousand and one (Tao) family are conserved throughout evolution. Three Tao proteins are encoded in the human genome (TAO1, TAO2, and TAO3), while

D. melanogaster possesses a single ancestral Tao kinase (Tao-1). Like Hpo and GckIII, Tao kinases belong to the Sterile 20-like kinase family. Tao kinases have been linked to multiple functions including control of organ growth and stem cell proliferation via the Hippo pathway (Boggiano et al., 2011; Poon et al., 2011; Poon et al., 2016), epithelial cell shape, animal behavior, and microtubule polymerization (Liu et al., 2010; King et al., 2011; Gomez et al., 2012). The substrates of Tao kinases, and thereby the mechanism by which they regulate these processes, are less well defined. Perhaps the best-characterized Tao-1 substrate is the Hpo kinase; Tao-1 activates Hpo by phosphorylating its activation loop, and this phosphorylation event is conserved in human cells between the orthologous kinases TAO1 and MST2 (Boggiano et al., 2011; Poon et al., 2011). Tao-1 can also activate the related Sterile 20-like kinase Misshapen in the *D. melanogaster* midgut (Li et al., 2018). When active, Hpo can phosphorylate the hydrophobic motif of the NDR family kinase Wts, which triggers Wts autophosphorylation and activation (Pan, 2010; Li et al., 2018). Likewise, the human Hpo orthologs MST1 and MST2 can phosphorylate and regulate the activity of the Wts orthologs LATS1 and LATS2 (Praskova et al., 2008).

The *D. melanogaster* respiratory system, or trachea, is composed of a simple epithelium arranged into tubes of three distinct architectures (Samakovlis et al., 1996). The smallest tubes form within the terminal cells of the tracheal system and are morphologically similar to the seamless endothelial tubes found in the vertebrate vascular system (Yu et al., 2015). Within terminal cells, there is a region termed the transition zone, wherein a tube containing an auto-cellular junction connects to a seamless tube. This seamless tube extends distally and branches dozens of times to ramify extensively on internal tissues where the tubes serve as the primary site of gas exchange. In prior studies, we determined that terminal cells lacking CCM3 or GckIII function show dramatic tube dilation within this transition zone (Song et al., 2013).

In humans, CCM3 is one of three genes known to be affected in cases of familial cerebral cavernous malformations. CCM3 binds to members of the GCKIII subfamily of Sterile 20-like kinases, of which there are three in humans (Draheim et al., 2014). The ability of CCM3 to bind GCKIII family members is thought to be essential to its function (Zalvide et al., 2013), and in flies, which have a single extant GCKIII family member, loss of GCKIII and CCM3 have identical consequences for the tracheal system (Song et al., 2013). Likewise, CCM3 and GCKIII have been shown to function together in zebrafish and nematodes (Yoruk et al., 2012; Zalvide et al., 2013; Lant et al., 2015). Despite much progress, the precise mechanism by which loss of CCM3 leads to tube dilation remains unknown, and likewise, the substrates of GCKIII family members in the vascular system remain mysterious.

Using protein affinity purification and mass spectrometry as an unbiased approach, we identified GckIII as a binding partner of Tao-1. Analogous to the way that Tao-1 activates Hpo, we found that Tao-1 phosphorylates and activates GckIII and that this relationship is conserved in human cells. Even more importantly, we show that Tao-1 and GckIII function together with the NDR family kinase Trc to regulate tube formation in trachea. Therefore, our study shows that Tao-1 regulates distinct biological processes by activating two related Hippo-like signaling modules containing a Sterile 20-like kinase and an NDR family kinase. The fact that Tao kinases regulate both organ growth and morphogenesis suggests that they could serve as key signaling nodes that couple both of these processes during organogenesis.

RESULTS

Tao-1 Binds to GckIII Kinase and Phosphorylates Its Activation Loop in *D. melanogaster* Cells

To identify potential targets of the Tao-1 kinase, we generated *D. melanogaster* S2 cell lines that stably expressed Tao-1 fused to an affinity tag at the N terminus (see STAR Methods). Tao-1 was affinity purified and subjected to mass spectrometry. Among the proteins retrieved with the highest abundance was the Sterile 20-like kinase GckIII. We identified 35 and 12 GckIII peptides in two independent experiments (0 peptides in six control samples), with a SAINT (Choi et al., 2011) probability of 1, indicating a highly significant interaction (Table S1).

We pursued potential regulatory links between Tao-1 and GckIII because, based on sequence homology, the GckIII kinase is most closely related to Hpo, another Sterile 20-like kinase that we and others previously discovered to be regulated by Tao-1 in the context of epithelial tissue growth (Poon et al., 2011; Boggiano et al., 2011). Initially, we confirmed that Tao-1 can form a physical complex with GckIII by performing co-immunoprecipitation experiments in *D. melanogaster* S2R+ cells. N-terminally tagged versions of hemagglutinin (HA)-Tao1 and myc-GckIII (both wild-type and kinase-dead versions for each) were co-expressed, followed by immunoprecipitation using anti-HA. This revealed that irrespective of their activity status, Tao-1 and GckIII can form a complex in *D. melanogaster* cells, as judged by the co-immunoprecipitation of both wild-type and kinase-dead variants (Figure 1A).

Next, considering that Tao-1 activates the closely related kinase Hpo by phosphorylating its T-loop (activation loop) (Boggiano et al., 2011; Poon et al., 2011), we tested whether Tao-1 can also phosphorylate GckIII. To do so, we pursued two lines of research. First, we examined the impact of Tao-1 expression on phosphorylation of the GckIII activation loop (Thr167, which is highly conserved between *D. melanogaster* and human orthologs [Figure 1B]) in S2R+ cells. Indeed, Thr167 phosphorylation of kinase-dead GckIII was substantially elevated upon co-overexpression of Tao-1 (Figure 1C). Second, we studied Tao-1-mediated *in vitro* phosphorylation of recombinant full-length kinase-dead GckIII. Consistent with our cell-based studies, expression of wild-type but not kinase-dead Tao-1 phosphorylated the activation loop of GckIII (Figure 1D). Collectively, these experiments suggest that Tao-1 can phosphorylate GckIII at residue Thr167 of its activation loop, a molecular event known to trigger the activation of Sterile 20-like kinases (Glantschnig et al., 2002; Deng et al., 2003).

TAO1 Binds to GCKIII Kinases in Human Cells and Phosphorylates Their Activation Loop

Considering that GCKIII is conserved between *D. melanogaster* and humans, and that the Tao-1/Hippo regulatory relationship is conserved between *D. melanogaster* and humans (Boggiano et al., 2011; Poon et al., 2011), we asked next whether human TAO1 interacts with and phosphorylates MST3, MST4, and/or

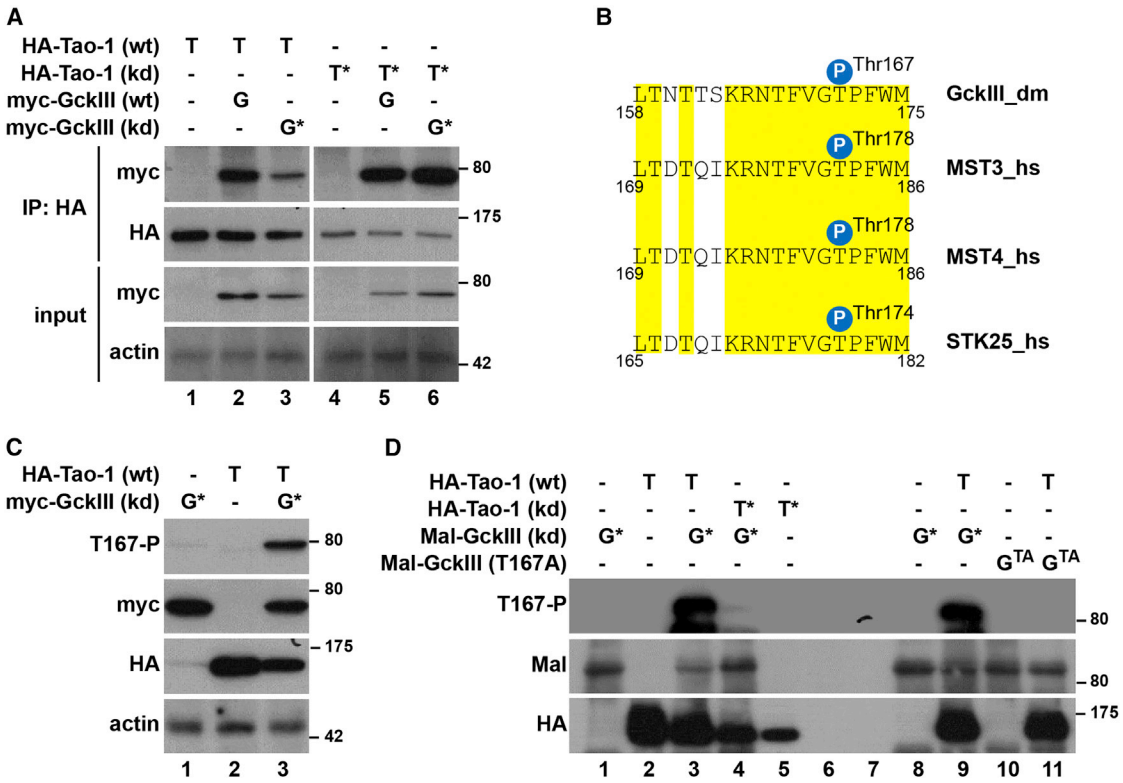

Figure 1. *D. melanogaster* Tao-1 Kinase Binds and Phosphorylates GckIII Kinase on Its Activation Loop

(A) Lysates of *D. melanogaster* S2R+ cells expressing wild-type (wt) or kinase-dead (kd) HA-Tao-1 together with wt or kd myc-GckIII were subjected to immunoprecipitation (IP) using anti-HA antibodies. Immunoprecipitates and input lysates were analyzed by immunoblotting with the indicated antibodies.

(B) Alignment of the conserved T-loop of *D. melanogaster* (dm) and human (hs) GCKIII kinase sequences. Identical residues are highlighted in yellow. The positions of the regulatory T-loop phosphorylation sites are indicated. The T-loop phosphorylation site of GCKIII kinases is conserved in flies and humans.

(C) S2R+ cells were transfected with the indicated plasmids and immunoblotted using anti-T167-P (top), anti-myc (top middle), anti-HA (bottom middle), and anti-actin (bottom) antibodies.

(D) Lysates of S2R+ cells transiently expressing HA-Tao-1 variants were subjected to immunoprecipitation with anti-HA antibodies. Immunopurified proteins were then used in kinase assays with or without the indicated recombinant versions of Mal-GckIII. Following kinase reactions, the samples were immunoblotted with the indicated antibodies. The anti-T167-P antibody specifically detected Tao1-mediated phosphorylation of GckIII on Thr167 (compare lanes 3, 9, and 11). Relative molecular masses are shown in kDa for each blot.

See also Table S1.

STK25, the three human counterparts of *D. melanogaster* GCKIII (hereafter, collectively termed hGCKIII) (Dan et al., 2001). The corresponding hGCKIII and TAO1 cDNAs were expressed in human HEK293 cells and TAO1/hGCKIII complex formation assessed by co-immunoprecipitation experiments. As shown in Figure 2A, TAO1 formed a complex with all three GCKIII homologs. These results are consistent with an unbiased high-throughput protein-protein interaction study that identified physical interactions between TAO1 and STK25, as well as TAO2 and STK25 (TAO2 is a homolog of TAO1) (Huttlin et al., 2015).

Subsequently, we investigated whether human TAO1 phosphorylates the activation loop of hGCKIII kinases in human cells and *in vitro*. We observed activation loop phosphorylation of hGCKIII in immunoprecipitates from cells that were co-transfected with TAO1 and hGCKIII kinases (Figure 2A). We observed similar results when assessing TAO1's ability to induce activation loop phosphorylation of endogenous hGCKIII (Figure 2B). Furthermore, this was dependent on TAO1's kinase activity as expression of kinase-dead TAO1 had no impact on hGCKIII activation loop phosphorylation (Figure 2B). In parallel, we performed *in vitro* kinase assays using recombinant full-length kinase-dead hGCKIII proteins as substrates. We observed hGCKIII activation loop phosphorylation by wild-type, but not kinase-dead, TAO1 immunoprecipitates (Figure 2C). Taken together, our data suggest that GckIII kinases are bona fide substrates of Tao kinases in both *D. melanogaster* and human cells.

GCKIII Does Not Regulate Tissue Growth via the Hippo Pathway

We next explored the biological setting in which Tao-1 regulates GckIII, by examining control of tissue growth by the Hippo pathway. Tao-1 controls epithelial tissue growth by activating the Hpo kinase by phosphorylating its activation loop (Boggiano et al., 2011; Poon et al., 2011). When active, Hpo phosphorylates the other members of the Hippo pathway core kinase cassette Salvador, Mats, and Wts (Pan, 2010; Harvey et al., 2013; Halder and Johnson, 2011). Wts phosphorylates the transcriptional co-activator protein Yorkie (Yki), thus limiting its access to the

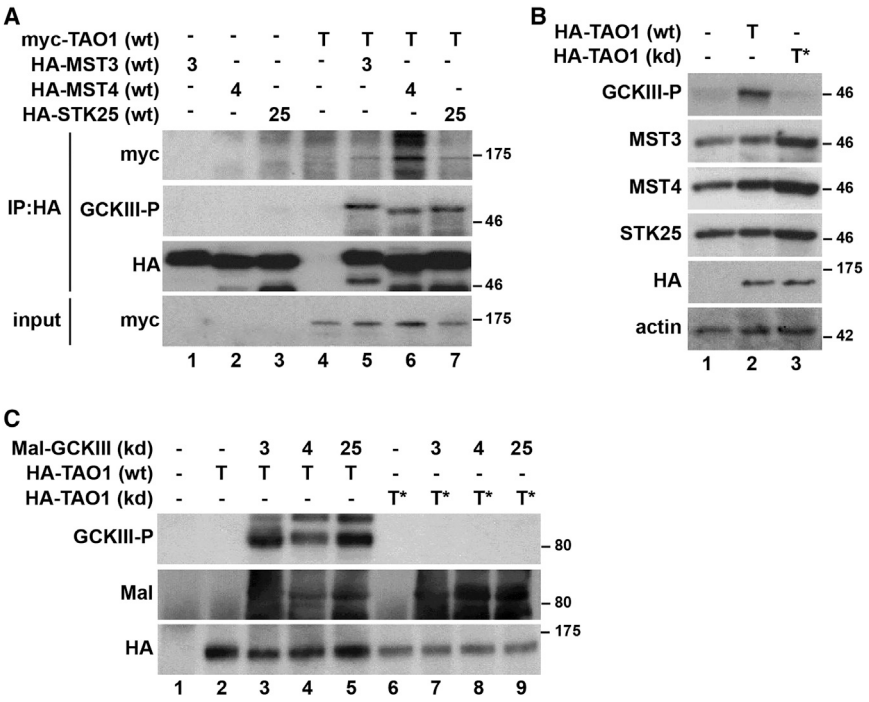

Figure 2. TAO1 Kinase Binds and Phosphorylates GCKIII Kinases on Their Activation Loop in Human Cells

(A) Lysates of human HEK293 cells expressing HA-GCKIII kinases (MST3, MST4, or STK25) together with myc-TAO1 were subjected to immunoprecipitation using anti-HA antibodies, before immunoblotting with the indicated antibodies.

(B) HEK293 cells expressing wt or kd human TAO1 were lysed and immunoblotted with the indicated antibodies.

(C) Lysates of HEK293 cells expressing human wild-type (wt) or kinase-dead (kd) HA-TAO1 were subjected to immunoprecipitation with anti-HA antibodies. Immunopurified kinases were used in kinase assays with or without the indicated recombinant wt or kd Mal-GCKIII kinases. Following kinase reactions, samples were examined by immunoblotting with the indicated antibodies. TAO1-mediated activation loop phosphorylation of human GCKIII kinases was observed only when wt TAO1 was incubated with kd GCKIII kinases. Relative molecular masses are shown in kDa for each blot.

nucleus and its ability to promote transcription of genes that promote tissue growth (Pan, 2010; Harvey et al., 2013; Halder and Johnson, 2011). Recently, Misshapen and Happyhour, which also belong to the Sterile 20-like kinase family, were shown to act in parallel to Hpo to promote Wts activity (Zheng et al., 2015; Meng et al., 2015; Li et al., 2014). Given that GckIII is the closest homolog of Hpo, we investigated the possibility that it also functions in parallel to Hpo to control Hippo pathway-dependent growth of epithelial tissues.

Initially, we assessed whether loss of *GckIII*, using either RNAi or mutant alleles, displayed tissue overgrowth, a characteristic feature of Hippo pathway genes (Tapon et al., 2002). Unlike the overgrown adult eyes harboring clones of *hpo* mutant tissue (Harvey et al., 2003; Pantalacci et al., 2003; Udan et al., 2003; Wu et al., 2003; Jia et al., 2003), *GckIII* mutant genetic mosaic adult eyes were rough and smaller in size than the control eyes (Figures S1A and S1B). Furthermore, depletion of *GckIII* by RNAi in the developing wing disc caused a reduction in the size of the adult wing, as opposed to overgrowth that might be expected should GckIII act similarly to Hpo (Figures S1C–S1E). Loss of Hippo pathway proteins causes Yki hyperactivation and elevated expression of DIAP1 (Huang et al., 2005). Using *hsFLP* MARCM (Lee and Luo, 1999), we generated GFP-marked clones in third instar larval wing imaginal discs that either harbored homozygous $hpo^{5.1}$ null (Genevet et al., 2009) mutant clones or expressed *GckIII* RNAi. However, *GckIII* depletion did not induce changes in DIAP1, as opposed to the increased DIAP1 expression observed upon loss of *hpo* (Figures S1F–S1G′). We considered the possibility that Hpo might compensate for GckIII in its absence and mask a role for GckIII in promoting Wts activity to limit tissue growth. To test this, we depleted *GckIII* by RNAi in $hpo^{5.1}$ null clones using the *eyFlp* MARCM system. The degree of tissue overgrowth was similar in adult eyes and head containing *hpo* null clones as it was in *hpo* null clones that also expressed a *GckIII* RNAi transgene (Figures S1H and S1I). Similar results were obtained when comparing the size of clones generated in third instar larval wing imaginal discs using the *hsFlp* MARCM system (Figures S1J–S1N). Therefore, we conclude that GckIII does not regulate Hippo pathway-dependent growth of epithelial tissues. These findings are consistent with recent biochemical studies of Zheng et al., who reported that, in contrast to Hpo, GckIII does not phosphorylate Wts or regulate its activity in *D. melanogaster* cultured cells (Zheng et al., 2015). To investigate the apparent undergrowth of *GckIII* mutant tissue, we assessed both cell proliferation and apoptosis in developing eye imaginal discs. While we observed no discernible change in cell proliferation (Figures S2A–S2D′) of *GckIII* mutant eye cells, we did observe an increased number of apoptotic cells (Figures S2E–S2H′) consistent with previous observations of *GckIII* depletion in the wing imaginal disc (Friedman and Perrimon, 2006). Collectively, this indicates that, unlike Hpo, GckIII does not normally suppress growth of eye or wing imaginal discs.

Tao-1 Kinase Regulates Tube Structure in *D. melanogaster* Trachea

We then investigated a role for Tao-1 in tracheal development, given that we had previously found that *GckIII* mutations lead to dilation of the tube within the terminal cell transition zone in larval trachea (Song et al., 2013). Three tube types are found in *D. melanogaster* trachea: multi-cellular, auto-cellular, and seamless tubes (Figure 3A). In trachea, terminal cells (composed of seamless tubes) connect to and branch out from stalk cells (composed of auto-cellular tubes) at an intercellular junction (arrow, Figure 3A′). The region positioned between the intercellular junction (arrow) and terminal cell nucleus is known as

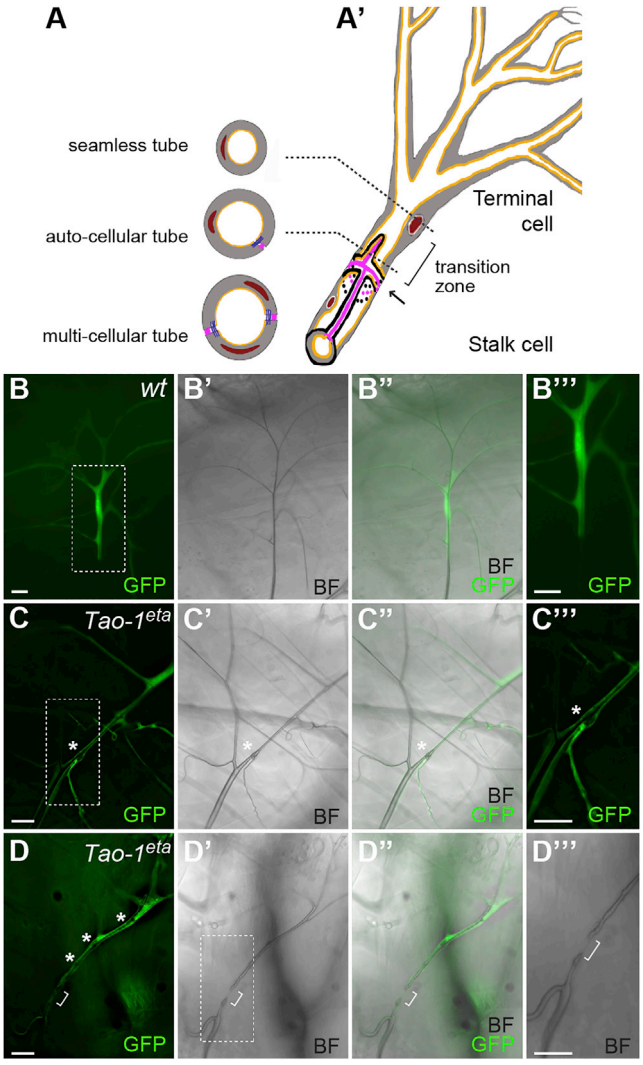

Figure 3. Tao-1 Regulates Development of *D. melanogaster* Trachea

(A and A′) Schematic illustration of *D. melanogaster* trachea, which comprise three different tube architectures: seamless tubes, auto-cellular tubes, and multi-cellular tubes (cross sections represented in (A). (A′) A depiction of part of a terminal cell (a seamless tube) that joins to an auto-cellular stalk cell at the transition zone (marked by bracket), which is located between an intracellular junction (marked by arrow) and the nucleus. Nucleus is brown; cytoplasm is gray; septate junctions are pink; adherens junctions are purple; apical lumens are orange (adapted from Song et al., 2013).

(B–D‴) Wild-type (B–B‴) or *Tao-1*^{eta} (C–D‴) terminal cell clones, marked by GFP (green). Boxed areas in (B), (C), and (D′) are shown as close-up images in (B‴), (C‴), and (D‴). Brightfield (BF) images are shown in (B′), (C′), (D′), and (D‴) and the merged images (B″), (C″), and (D″). (B–B‴) Gas-filled tubes that pierce the cytoplasm are evident in the wild-type terminal cell. The tube extends beyond the clone through the unmarked neighboring stalk cell. (C–C‴) Loss of *Tao-1* results in prominent dilations (*) in the transition zone of 73% of terminal cells scored (D–D‴) A *Tao-1*^{eta} terminal cell clone that displays a "gap" defect, in which a portion of the terminal cell tube is absent within the transition zone (bracket). The cell also displays several small tube dilations (marked by *). Scale bars, 20 μm.

See also Figures S1–S3 and Table S2.

the transition zone (bracket, Figure 3A′), to reflect the transition from seamed to seamless tubes (Song et al., 2013; Samakovlis et al., 1996). We generated *Tao-1* loss-of-function clones in trachea using the *hsFLP*-GFP system (Ghabrial et al., 2011) and the *Tao-1*^{eta} allele (Gomez et al., 2012). Strikingly, we observed transition zone tube dilation in 73% of terminal cells and transition zone tube gaps (or restrictions) in 26% of terminal cells (1 terminal cell showed both a local dilation and a gap) (Figures 3B–3D‴ and Table S2). We also observed small bulges in the seamless tubes of multiple tracheal terminal cells (Figures 3D–3D‴), consistent with the *GckIII* loss-of-function phenotype we reported previously (Song et al., 2013).

To confirm these results, we used two independent Tao-1 RNAi lines that we have previously employed to deplete this protein in epithelial tissues and neural stem cells (Poon et al., 2011, 2016). Similar to what we observed using the classical loss-of-function allele, when Tao-1 was depleted by RNAi in trachea using *btl-GAL4*, we observed transition zone dilations (Figures S3A–S3A‴). Transition zone dilations were observed in 74% of *Tao-1* RNAi-expressing terminal cells, transition zone gaps in 12% of terminal cells, and no gross morphological defects in 14% of terminal cells (n = 34) (Figures S3A–S3B‴ and Table S2). Furthermore, we assessed *hpo*$^{42–47}$ mutant clones in trachea and observed no dilations in terminal cells (either in transition zones or terminal cell branches; Figures S3C–S3C‴ and Table S2) suggesting that Tao-1 and Hippo perform distinct functions in tracheal development. Collectively, these data show that Tao-1 is an essential regulator of tracheal development and that Tao-1 loss largely phenocopies *GckIII* loss in this tissue.

Tao-1 Regulates the Abundance and Localization of Junctional and Apical Proteins in Trachea

Given our biochemical evidence that Tao-1 binds to and activates GckIII and that loss of either *Tao-1* or *GckIII* causes transition zone dilation in trachea, we asked whether loss of *Tao-1* results in abnormal localization of junctional and apical proteins, as was reported for *Ccm3* and *GckIII* mutants (Song et al., 2013). The transition zone of wild-type trachea contains septate and adherens junctions in the proximal part of the terminal cell (Song et al., 2013; Samakovlis et al., 1996). This small stretch of auto-cellular tube in terminal cells is frequently remodeled away by the third larval instar, but it tends to persist in *Ccm3* and *GckIII* mutant cells and is evident by ectopic expression of septate junction proteins (Song et al., 2013). We observed a similar perdurance of auto-cellular junctions in *Tao-1* mutant terminal cells, which displayed ectopic expression of septate junction proteins such as Fasciclin 3 (Fas 3) and Varicose (Vari) (arrowheads in Figures 4A–4D″).

In *Ccm3* and *GckIII* mutant terminal cells, the apical membrane protein Crumbs, which is normally present only in discrete puncta along the apical membranes of the terminal cell, accumulates at high levels on these membranes (Figures 4E–4E′; Song et al., 2013). Compared to Crumbs-GFP localization in wild-type terminal cells, Crumbs-GFP was more highly expressed and lined the majority of the apical lumen of terminal cells expressing *Tao-1* RNAi (Figures 4F–4F′). These data strongly suggest a common molecular defect underlies the transition zone dilation caused by loss of either *GckIII* or *Tao-1*.

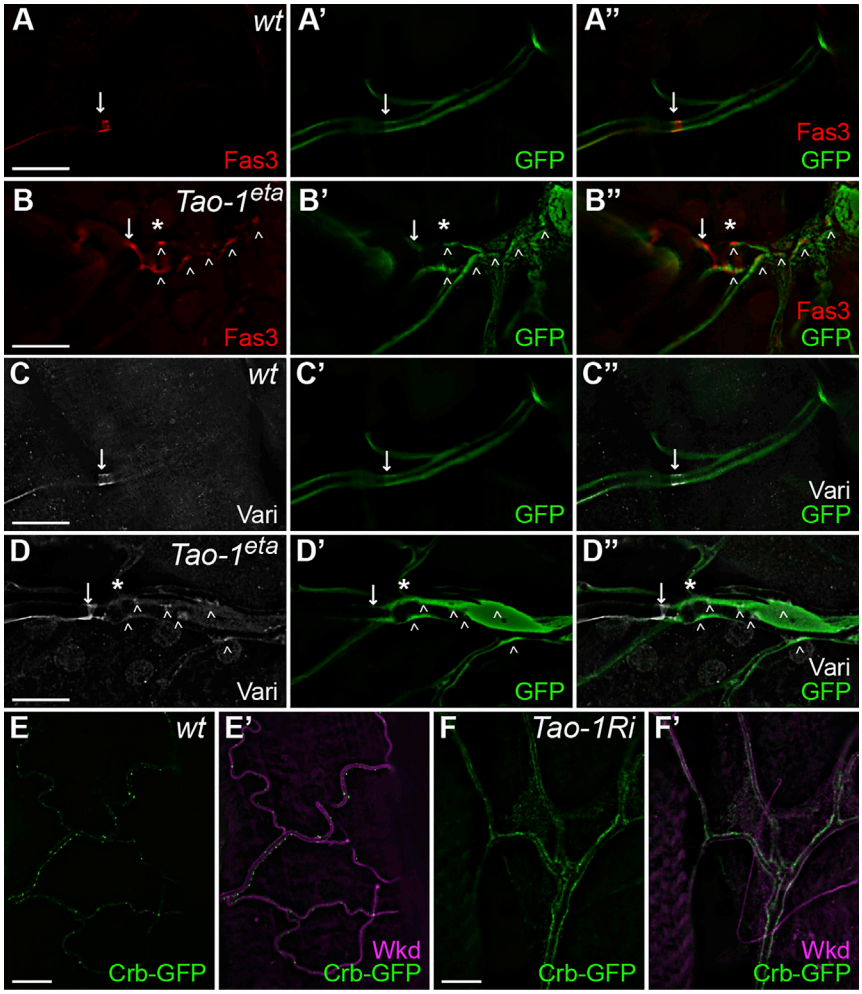

Figure 4. Tao-1 Prevents Ectopic Accumulation of Septate Junction Proteins and Crumbs in Trachea

(A–D″) Terminal cell clones of the indicated genotypes marked by GFP and stained for antibodies specific for Fas3 (red) or Varicose (white). The arrow indicates the intercellular junction. (A–A″) and (C–C″) are from the same double stained terminal cell clone. In wild-type terminal cell GFP-positive clones (green), Fas3 (A–A″, red) and Varicose (C–C″, white) are expressed at the septate junction of the autocellular tube and at the intercellular junction (arrow). In comparison, in *Tao-1*^{eta} terminal cell clones, ectopic Fas3 (B–B″, red) and ectopic Vari (D–D″, white) are observed in the transition zone dilation (indicated by *) and in more distal positions of the cell (indicated by arrowheads, B and D).

(E and F′) Terminal cells with Crumbs-GFP (green) stained with antibodies specific for Wkd (magenta) to mark tracheal tubes. In wild-type terminal cells (E–E′), Crumbs-GFP (green, E–E′) decorates the lumenal membrane (Wkd, magenta, E′) in well-spaced foci. In comparison, in terminal cells expressing *Tao-1 RNAi* with *btl-Gal4* (F–F′), Crumbs-GFP levels (green, F–F′) were elevated and appeared to almost continuously line the lumenal membrane (marked by Wkd, magenta, F–F′).

Scale bars, 20 μm.

Tao-1 Functions Upstream of GckIII to Control Tracheal Morphogenesis

Coupled with the finding that Tao-1 forms a complex with GckIII and phosphorylates the GckIII activation loop (Figures 1 and 2), our observations are consistent with the notion that these proteins operate together to control tracheal morphogenesis. To investigate this further, we assessed the epistatic relationship between Tao-1 and GckIII *in vivo*. We used the MARCM system to generate tracheal terminal cells that were mutant for *GckIII*, using a *GckIII*^{wheezy} molecular null mutant allele (Song et al., 2013), and also expressed a hyperactive Tao-1 allele (*Tao-1*^{HA}), where a central inhibitory domain had been removed (Liu et al., 2010) (Figure 5A). Expression of *Tao-1*^{HA} in terminal cells using *drm>GFP* had no discernible phenotype (Figures S3A–S3A‴ and Table S2) and failed to rescue the transition zone dilations associated with the *GckIII*^{wheezy} allele, consistent with Tao-1's operating upstream of GckIII (Figures 5B–5C″ and Table S2). We tested this further by utilizing a hyperactive GckIII transgene (*GckIII*^{HA}), where the activation loop residue at position 167 was mutated from threonine to aspartic acid, which mimics phosphorylation of this residue (Figure 5A). Expression of *GckIII*^{HA} alone largely causes a mild wavy lumen phenotype (Figure S4B and Table S2), and co-expression of *GckIII*^{HA} in *Tao-1*^{eta} mutant terminal cells partially rescued phenotypes associated with *Tao-1* loss, including dilation of the transition zone (Figures 5D–5D″ and Table S2). Phosphorylation at T167 is essential for GckIII function since expression of a mutant version of GckIII (*GckIII*^{T167A}), where T167 is mutated to alanine thus rendering this site unable to be phosphorylated, resulted in dilations in 66% of terminal cells scored (Figures 5E–5E″ and Table S2). Together with our biochemical data (Figures 1 and 2), these epistasis studies indicate that GckIII functions downstream of Tao-1 in tracheal terminal cells.

GCKIII Phosphorylates the Hydrophobic Motif of Tricornered to Regulate Tracheal Development

Given the architecture of Hippo-like signaling modules, we predicted that an NDR family kinase would operate downstream of GckIII in trachea. *D. melanogaster* has two such kinases: Wts and Trc. We considered Trc to be the lead candidate because of two prior results obtained by our groups: (1) the human GCKIII ortholog MST3 phosphorylates the hydrophobic motif of the human Trc orthologs, NDR1 and NDR2, an essential step in their activation (Stegert et al., 2005; Cornils et al., 2011), and this motif is conserved in Trc/NDR kinases in flies and humans (Figure 6A); and (2) *wts* mutant trachea display overgrowth phenotypes (Ghabrial et al., 2011), which are distinct from the tracheal dilations observed upon *GckIII* or *Tao-1* loss (Song et al., 2013) (Figures 3C and 5B).

Initially, we sought to determine whether the reported biochemical relationship between hGCKIII and NDR1/2 was conserved between the *D. melanogaster* and human orthologs.

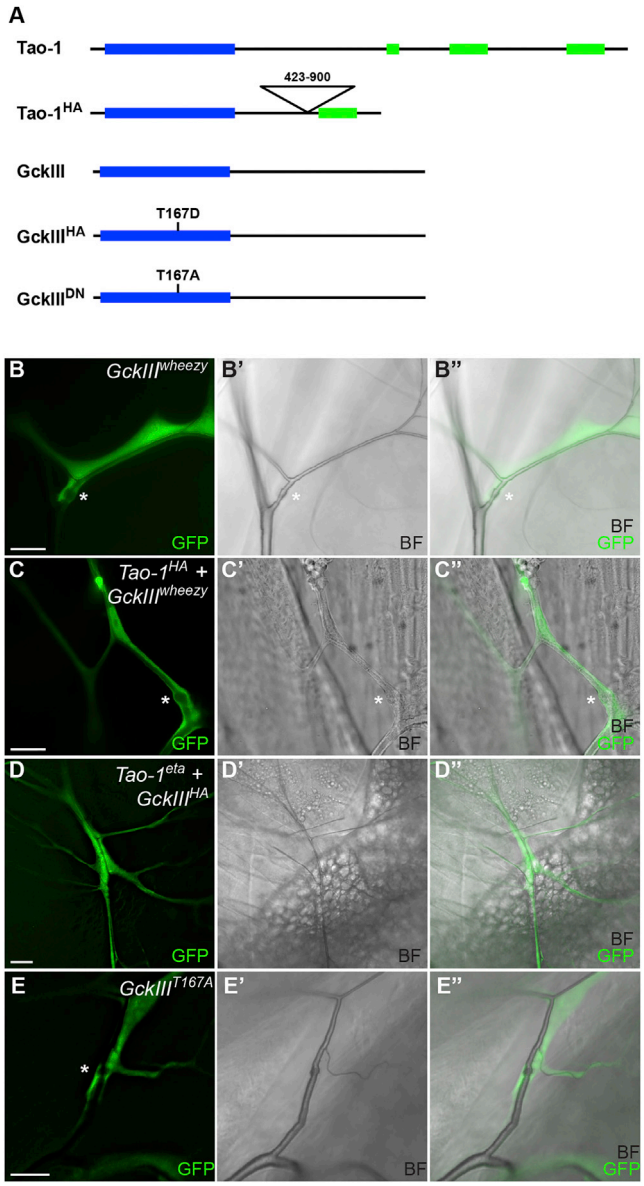

Figure 5. GckIII Functions Epistatically to Tao-1 in Trachea

(A) Schematic of Tao-1 and GckIII wild-type and mutant transgenes utilized for genetic epistasis experiments. Blue boxes indicate a kinase domain, and green boxes indicate coiled-coil domains. Wild-type Tao-1 contains a kinase domain at the N terminus and 3 coiled-coil domains at the C terminus. Hyperactive Tao-1 (Tao-1^{HA}) contains a deletion in the central region (amino acids 423–900). Wild-type GckIII contains a kinase domain at the N terminus; hyperactive GckIII (GckIII^{HA}) contains a point mutation where T is mutated to D to mimic phosphorylation at 167 in the activation loop of the kinase domain; and dominant negative GckIII (GckIII^{DN}) contains a point mutation where T is mutated to A to prevent phosphorylation at 167 in the activation loop of the kinase domain.

(B–E) Terminal cell clones of the indicated genotypes are marked by GFP (green) with accompanying brightfield (BF) images. Transition zone tube dilations are marked by an asterisk (*).

(B–B″) *GckIII^{wheezy}* terminal cell clones, marked by GFP (green). Transition zone tube dilations (*) are observed in 100% of *GckIII^{wheezy}* mutant clones scored.

(C–C″) A *GckIII^{wheezy}* terminal cell clone (marked by GFP) expressing a hyperactive *Tao-1 (Tao-1^{HA})* transgene. Expression of hyperactive *Tao-1* failed to rescue transition zone dilations in *GckIII^{wheezy}* mutant cells, and transition zone tube dilations were observed in 100% of terminal cells scored.

(D–D″) A *Tao-1^{eta}* terminal cell clone (marked by GFP) expressing a hyperactive *GckIII (GckIII^{HA})* transgene. Expression of hyperactive *GckIII^{HA}* in *Tao-1^{eta}* mutant clones caused transition zone tube dilations in 51% of terminal cells scored.

(E–E″) Expression of a *GckIII* transgene bearing the point mutation T167A in the activation loop (*GckIII^{T167A}*) results in transition zone tube dilations in 66% of terminal cells scored.

Scale bars, 20 μm.

See also Figure S4 and Table S2.

Lysates of S2R+ cells transiently expressing wild-type or kinase-dead GckIII were subjected to immunoprecipitation with anti-HA antibodies, and immunopurified proteins were incubated with the recombinant Mal-tagged hydrophobic motif fragment of Trc. Following *in vitro* kinase reactions, samples were examined by immunoblotting, using antibodies that detect phosphorylation of the hydrophobic motif of Trc (Thr449). We observed robust phosphorylation of this residue (Figure 6B), showing, for the first time in *D. melanogaster*, that GckIII can phosphorylate the hydrophobic motif of Trc and suggesting that this regulatory relationship is conserved between flies and mammals. To determine whether phosphorylation was direct as opposed to an intermediate kinase, we performed *in vitro* kinase assays using recombinant human kinases (NDR1 and NDR2 as substrates and MST1-4 and STK25 as kinases). We found that all three human GCKIIIs (MST3, MST4, and STK25) as well MST1 and MST2 (the human Hpo orthologs) can phosphorylate human NDR1 and NDR2 to differing degrees on Thr444 and Thr442 (Figure 6C), their respective hydrophobic motif phosphorylation sites that are essential for NDR1/2 activation (Hergovich, 2013, 2016). Taken together, our data show that Trc/NDR kinases are substrates of GCKIII kinases in both flies and humans.

To investigate the function of Trc in trachea, we used *drm-GAL4* to express *trc* RNAi transgenes or examined clones of the classic *trc^{1}* allele (Geng et al., 2000) in trachea terminal cells. Strikingly, we observed tracheal dilation phenotypes in the transition zone of *trc^{1}* terminal cells (98% of 44 terminal cell clones examined; Figures 6D–6D″ and Table S2), which closely phenocopied those observed upon loss of either *GckIII* or *Tao-1*. Consistently, expression of *trc* RNAi under control of *drm-GAL4* at 29°C induced a high frequency of transition zone dilations, while a small number of tubes also displayed a gap defect in the transition zone (Table S2 and Figure S5). All terminal cells mutant for *trc* or expressing *trc* RNAi were also defective in gas filling (Figures 6D–6D″ and Table S2). Gas-filling defects are frequently found among mutations affecting terminal cell morphology, and similar gas-filling defects were seen at a very low frequency in *GckIII* mutant terminal cells (Ghabrial et al., 2011). As with terminal cells mutant for either *GckIII* or *Tao-1*, we observed ectopic expression of different septate junction proteins upon RNAi-mediated depletion of *trc*. In *drm-GAL4, trc RNAi* terminal cells, ectopic Fas3 expression was evident (Figures 6E–6E″), as was ectopic Coracle staining (Figures 6F–6F″), and similar data were observed in *trc^{1}* clones (data not shown). Upon *trc* depletion, we also observed substantial elevation of Crumbs-GFP expression, which lined the majority of the lumen of *trc RNAi* terminal cells (Figures 6G–6G″). Consistent with Trc acting downstream of GckIII in trachea, expression

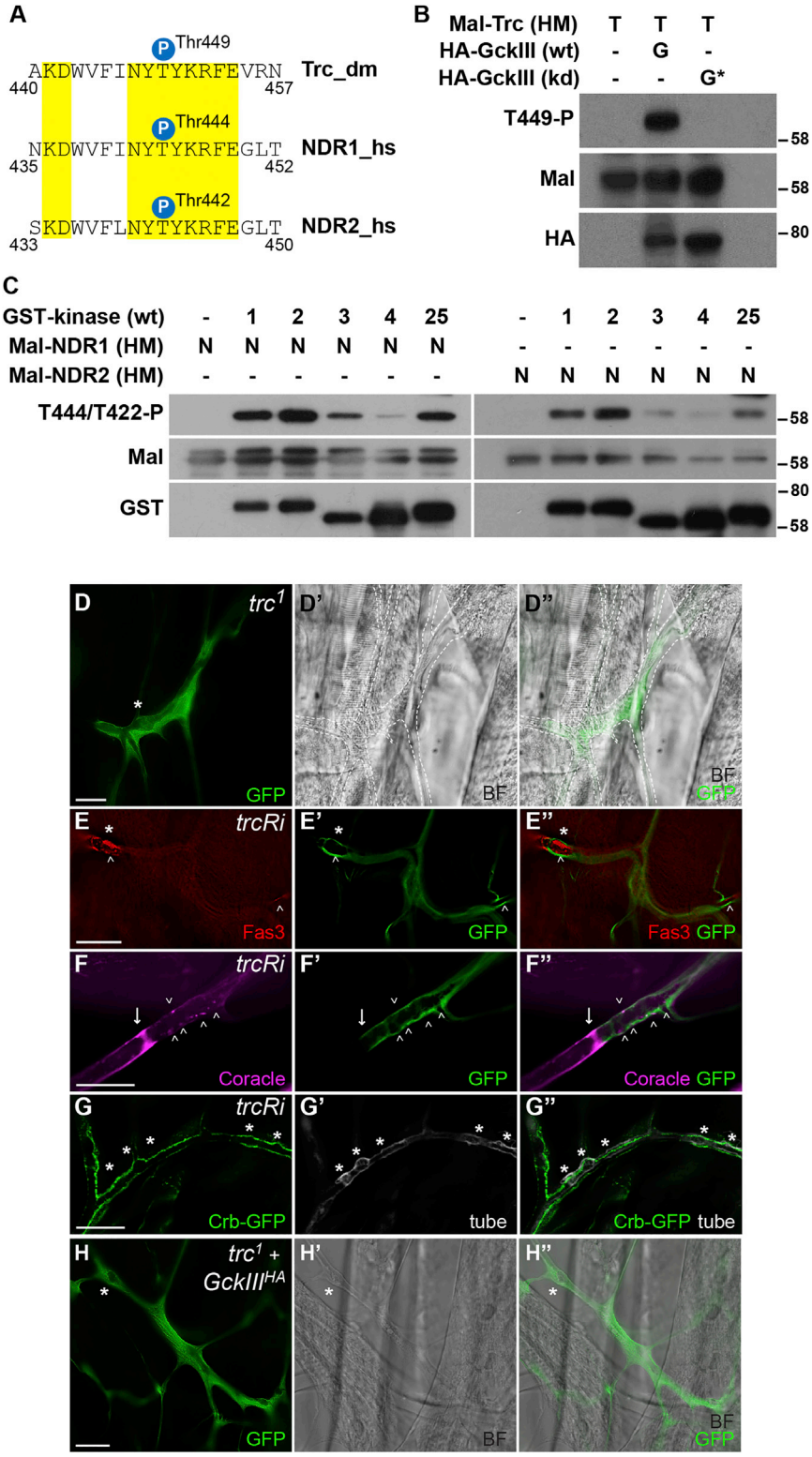

Figure 6. The Tricornered Kinase Is Phosphorylated on Its Hydrophobic Motif by GckIII and Regulates Tracheal Development

(A) Alignment of the hydrophobic motif of *D. melanogaster* (dm) and human (hs) NDR kinase sequences. Identical residues are highlighted in yellow. The positions of the regulatory hydrophobic motif phosphorylation sites are indicated. The hydrophobic motif phosphorylation site of Trc/NDR kinases is conserved from flies to humans.

(B) Lysates of S2R+ cells transiently expressing wild-type (wt) or kinase-dead (kd) HA-GckIII were immunoprecipitated with anti-HA antibodies and incubated with a recombinant Mal-tagged hydrophobic motif fragment of Trc (Mal-Trc[HM]) in kinase assays. Subsequently, samples were examined by immunoblotting using the indicated antibodies. Relative molecular masses are shown in kDa for each blot.

(C) Recombinant glutathione S-transferase (GST)-tagged wild-type full-length MST kinases (MST [1], MST2 [2], MST3 [3], MST4 [4], or STK25 [25], with respective abbreviations in square brackets) were incubated with recombinant Mal-tagged hydrophobic motif fragments of human NDR1 or NDR2 (Mal-NDR1/2 [HM]). Following kinase reactions, the samples were analyzed by western blotting using the indicated antibodies. Relative molecular masses are shown in kDa for each blot.

(D–D″) A *trc*^{1} terminal cell clone marked by GFP (green). Brightfield (BF) images are shown in (D′) and the merged image (D″). The * indicates a prominent transition zone dilation. The terminal cell also exhibits a gas-filling defect and is outlined with a white dashed line in (C′) and (C″).

(E–E″) Terminal cell expressing a *trc RNAi* (*trcRi*) transgene using *btl-GAL4* (marked by GFP) and stained for Fas3 (red). Large dilations (*) in the transition zone were readily detected, and ectopic Fas3 is present in the transition zone dilation (arrowheads) of *Tao-1*^{eta} terminal cell clones and more distally as well (arrowheads).

(F–F″) Terminal cells marked with GFP (green) expressing a *trc RNAi* (*trcRi*) transgene using *drm-GAL4* and stained for Coracle (magenta) displayed ectopic localization of Coracle in the transition zone (arrowheads) and distally (data not shown). Arrows mark intercellular junction.

(G–G″) Terminal cell (tubes visualized with UV) expressing a *trc RNAi* (*trcRi*) transgene using *drm-GAL4* with Crumbs-GFP almost continuously lined the lumenal membrane.

(H–H″) A *trc*^{1} terminal cell clone (marked by GFP [green]) expressing a hyperactive *GckIII* transgene. A brightfield (BF) image is shown in (H′) and the merged image (H″). The * indicates a transition zone tube dilation; expression of hyperactive *GckIII* failed to rescue transition zone dilations in *trc*^{1} cells.

Scale bars, 20 μm in (D)–(H).

See also Figure S5 and Table S2.

of GckIII^{HA} in *trc*^{1} clones did not rescue the tube dilation defect (Figures 6H–6H″ and Table S2).

Next, we assessed Trc activity in trachea using the antibody that detects phosphorylation in the hydrophobic motif of hNDR kinases, a well-established readout to monitor the activity status of human NDR1/2 (Hergovich, 2013). Specifically, we utilized an antibody raised against the phosphorylated Thr444 site of NDR1 (Tamaskovic et al., 2003), which recognizes the equivalent site

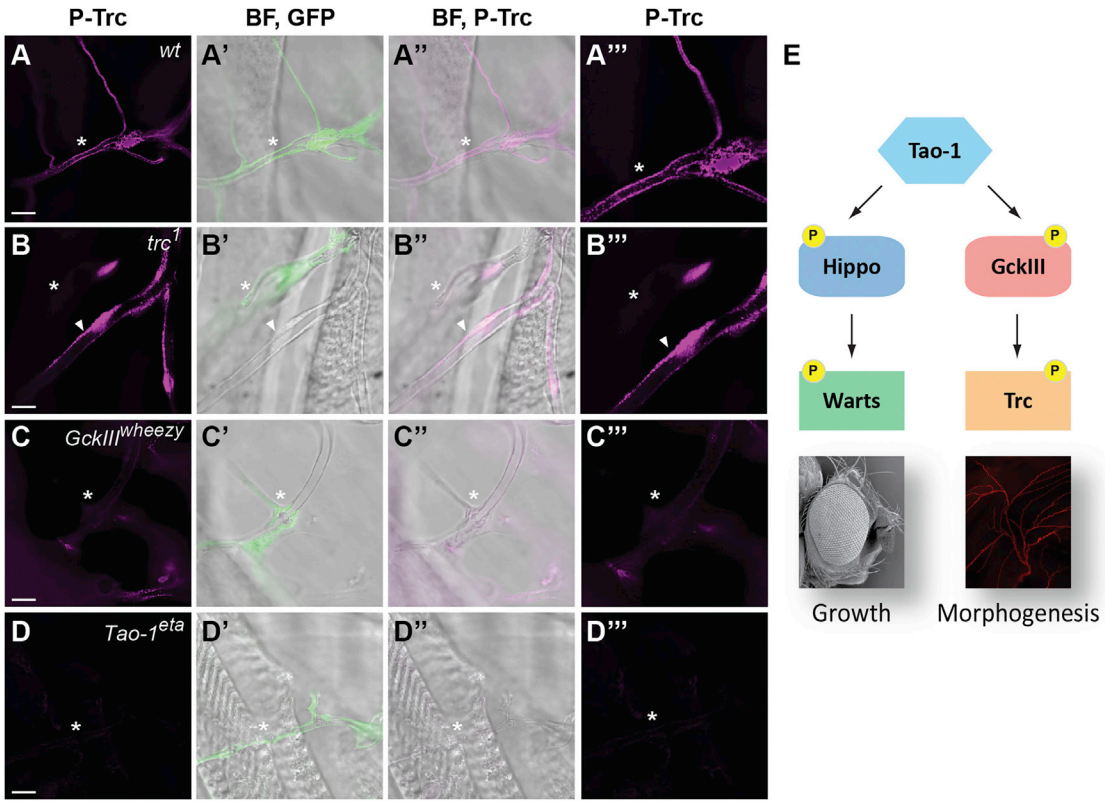

Figure 7. Tricornered Activity in Trachea Requires Tao-1 and GckIII

(A–D) Third instar larval trachea stained with antibodies that recognize phosphorylation of the activation loop of Trc (P-Trc). GFP positive terminal cells are shown of the following genotypes: (A–A‴) wild-type; (B–B‴) *trc*^{1}; (C–C‴) *GckIII*^{wheezy}; (D–D‴) *Tao-1*^{eta}. P-Trc is in magenta (A–D). Clones are marked by GFP (green) in panels merged with brightfield images (A′, B′, C′, and D′). P-Trc (magenta) is merged with brightfield images (A″, B″, C″, and D″). Close-up images of P-Trc (magenta) are shown in (A‴), (B‴), (C‴), and (D‴). GFP positive terminal cells are indicated by arrowheads. P-Trc is evident in puncta that line the apical membrane of wild-type and control tracheal lumens. P-Trc staining is reduced or absent in trachea that are mutant for *trc*, *GckIII* or *Tao-1* in (B)–(D). In (B)–(B‴), the asterisk indicates a control GFP negative terminal cell that stains positive for P-Trc and serves as an internal control. Scale bars, 10 μm.

(E) Tao-1 regulates two Hippo-like signaling modules. In addition to regulating Hippo-Warts signaling in organ growth, we have discovered that Tao-1 kinase regulates a related Hippo-like pathway consisting of GckIII and Trc in morphogenesis.

in *Drosophila* Trc, phosphorylated Thr449 (denoted herewith as P-Trc). In wild-type trachea, P-Trc was evident in puncta lining the apical membranes of terminal cells (Figures 7A–7A‴). Importantly, this is the region where phenotypes caused by loss of *Tao-1*, *GckIII*, or *trc* manifest, e.g., tube dilation and accumulation of septate junction proteins and Crumbs. To confirm the specificity of this signal, we stained *trc*^{1} mutant trachea and found complete absence of this signal in GFP-positive *trc*^{1} mutant cells (asterisk, Figures 7B–7B‴). As an internal control for this experiment, a wild-type terminal cell that neighbored the *trc*^{1} cell showed robust P-Trc staining (arrowhead, Figures 7B–7B‴). To determine whether Trc activity was dependent on Tao-1 and GckIII, we stained tracheal clones that were mutant for each of these genes. As shown in Figures 7C–7D‴, P-Trc signal was greatly reduced or undetectable in *Tao-1*^{eta} or *GckIII*^{wheezy} terminal cells. These results are consistent with our genetic epistasis experiments, which show that Trc functions downstream of Tao-1 and GckIII to control tracheal morphogenesis (Table S2). Collectively, our genetic and biochemical data indicate that we have identified a Hippo-like pathway, consisting of the Tao-1, GckIII, and Trc kinases, that regulates tracheal development in *D. melanogaster*.

DISCUSSION

Using genetic and biochemical experiments, we have defined Tao-1 as a kinase that acts at the apex of two ancient and closely related kinase modules that consist of a Sterile 20-like kinase and an NDR family kinase: Hpo and Wts; and GckIII and Trc (Figure 7E). Despite being similarly organized, Hippo-like kinase modules execute distinct functions downstream of Tao-1. While Hpo and Wts regulate organ size and cell fate, GckIII and Trc regulate the architecture of trachea. Presumably, these differences can be explained by the substrates of the downstream kinases in these signaling modules, Wts and Trc. A key step in defining how Hpo and Wts regulate organ size was the discovery that Wts phosphorylates the Yki transcription co-activator and inhibits its nuclear access (Huang et al., 2005). Identifying the substrate(s) of Trc is likely to offer similar mechanistic insights into how the Hippo-like pathway of Tao-1/GckIII/Trc regulates tracheal morphogenesis.

Of the many thousands of mutations analyzed in tracheal terminal cells, less than a handful affect tube morphology specifically in the transition zone (Baer et al., 2007; Beitel and Krasnow,

2000; Förster et al., 2010; Ghabrial et al., 2011; Myat et al., 2005; Ruiz et al., 2012; Samakovlis et al., 1996). Among these we have previously described mutations in *lotus*, which causes a local transition zone tube discontinuity or gap, and mutations in *GckIII* and *Ccm3*, which cause a local transition zone tube dilation (Song et al., 2013). Intriguingly, mutations in *Tao-1* cause both defects. The only other genetic condition reported to have this effect on terminal cell tubes is the combination of *GckIII* loss of function and knockdown of the septate junction protein, Varicose/PALS2 (Song et al., 2013). As in this case, loss of *Tao-1* appears to both compromise GckIII activity and septate junction formation, given that *Tao-1* mutant tracheal cells exhibit transition zone dilation and mislocalization of septate junction proteins. These data suggest that Tao-1 performs at least two functions to control tracheal morphology: (1) it acts upstream of GckIII and Trc to prevent transition zone tube dilation; and (2) it is required to maintain the integrity of septate junctions. Trc appears to be the key substrate of GckIII, based on our biochemical data and that the *trc* loss-of-function phenotype closely phenocopies GckIII loss in trachea. Indeed, the *trc* tube dilation phenotype is, if anything, more severe than for *Ccm3* or *GckIII*, with *trc* mutant terminal cells often exhibiting multiple large dilations in the transition zone. This would be consistent with residual Trc activity in *GckIII* mutant backgrounds, suggesting that additional Sterile-20 like kinases to GckIII may regulate Trc activity in terminal tracheal cells. If so, this would parallel regulation of *D. melanogaster* Wts and human LATS1 and LATS2 in the Hippo pathway, where multiple Sterile-20 kinases have been found to operate upstream of these NDR family kinases (Meng et al., 2015; Zheng et al., 2015; Li et al., 2014; Li et al., 2018).

In *D. melanogaster*, Trc also regulates polarized cell growth that underpins hair and bristle development (Geng et al., 2000) and tiling and branching of PNS dendrites (Emoto et al., 2004). It will be interesting to determine whether Trc regulates the same or similar proteins to control these different biological processes or whether it regulates multiple proteins, akin to Wts, which regulates Yki in the context of organ growth and R8 cell fate choice, and the actin regulatory protein Enabled to control border cell migration in the *D. melanogaster* ovary (Lucas et al., 2013; Huang et al., 2005; Jukam et al., 2013). Furthermore, it will be important to determine whether Tao-1 and GckIII operate upstream of Trc in other biological settings. In addition to discovering the key substrate(s) of Trc in trachea, defining modes of upstream regulation of Tao-1 activity should provide insights into how this Hippo-like signaling module controls tube development. One candidate upstream regulator is Schip1, which has been linked to Tao-1 and the Hippo pathway in the context of organ size control (Chung et al., 2016), although the mechanism by which it functions is unclear.

Previous findings by our group and others in both insects and vertebrates established the human orthologs of GckIII (MST3, MST4, and STK25) as potential disease genes in cerebral cavernous malformation, a familial vascular syndrome characterized by dilated leaky blood vessels (Song et al., 2013; Draheim et al., 2014). hGCKIII kinases bind to the non-catalytic protein CCM3, which is thought to serve as a scaffold for them. Theoretically, CCM3 could promote the association of GCKIII kinases with TAO kinases and/or NDR family kinases to facilitate their ability to phosphorylate one another and become active. This requires further examination, but our findings raise the possibility that the Tao-regulated Hippo-like signaling module identified here is required for proper blood vessel formation in humans and that aberrant activity of this module could contribute to cerebral cavernous malformation syndrome. If so, then our study could provide potential therapeutic targets for treatment of this disease.

STAR★METHODS

Detailed methods are provided in the online version of this paper and include the following:

- KEY RESOURCES TABLE
- CONTACT FOR REAGENT AND RESOURCE SHARING
- EXPERIMENTAL MODEL AND SUBJECT DETAILS
- METHOD DETAILS
  - *D. melanogaster* Stocks
  - Generation of Clones in *Drosophila*
  - Immunofluorescence
  - Cell Proliferation Assay
  - Transient Transfections of Cultured Cells
  - Expression Plasmids
  - Immunoblotting, Immunoprecipitations, and Antibodies
  - Mass Spectrometry
  - Kinase Assays
- QUANTIFICATION AND STATISTICAL ANALYSIS

SUPPLEMENTAL INFORMATION

Supplemental Information includes five figures and two tables and can be found with this article online at https://doi.org/10.1016/j.devcel.2018.09.024.

ACKNOWLEDGMENTS

We thank P. Adler, V. Riechmann, N. Tapon, E. Knust, the Vienna Drosophila RNAi Center, the Australian Drosophila Research Support Facility (www.ozdros.com), the Bloomington Drosophila Stock Center, and the Developmental Studies Hybridoma Bank for *D. melanogaster* stocks and antibodies. We thank the Centre for Advanced Histology and Microscopy at the Peter MacCallum Cancer Centre. H. Zhao provided help with SAINT analysis. K.F.H. is a National Health and Medical Research Council Senior Research Fellow (1078220). A.V. was supported by a grant from the National Institutes of Health (GM123136). Y.K. was sponsored by the Ministry of National Education (The Republic of Turkey). This research was supported by the Peter MacCallum Cancer Foundation and grants from the National Health and Medical Research Council of Australia (K.F.H. – 1032251 and C.L.C.P. – 1142469), the Company of Biologists (Development Journal) Travelling Fellowship (C.L.C.P.) (Harvey laboratory), the National Institutes of Health (1R01GM089782), the American Cancer Society (ACS) (RSG 124720) (Ghabrial laboratory), the Wellcome Trust (090090/Z/09/Z), and BBSRC (BB/I021248/1) (Hergovich laboratory).

AUTHOR CONTRIBUTIONS

Conceptualization, C.L.C.P., A.G., and K.F.H.; Methodology, C.L.C.P., A.V., A.H., A.G., and K.F.H.; Investigation, C.L.C.P., W.L., Y.S., M.G., Y.K., X.Z., W.X., and A.G.; Formal Analysis, C.L.C.P., W.L., Y.S., and A.G.; Writing – Original Draft, C.L.C.P., A.G., and K.F.H.; Supervision, A.V., A.H., A.G., and K.F.H.; Funding Acquisition, C.L.C.P., A.V., A.H., A.G., and K.F.H.

DECLARATION OF INTERESTS

The authors declare no competing interests.

Received: September 19, 2017
Revised: August 26, 2018
Accepted: September 28, 2018
Published: October 25, 2018

REFERENCES

Avruch, J., Zhou, D., Fitamant, J., Bardeesy, N., Mou, F., and Barrufet, L.R. (2012). Protein kinases of the Hippo pathway: regulation and substrates. Semin. Cell Dev. Biol. *23*, 770–784.

Bachmann, A., Draga, M., Grawe, F., and Knust, E. (2008). On the role of the MAGUK proteins encoded by Drosophila varicose during embryonic and postembryonic development. BMC Dev. Biol. *8*, 55.

Baer, M.M., Bilstein, A., and Leptin, M. (2007). A clonal genetic screen for mutants causing defects in larval tracheal morphogenesis in Drosophila. Genetics *176*, 2279–2291.

Bardin, A.J., and Amon, A. (2001). Men and sin: what's the difference? Nat. Rev. Mol. Cell Biol. *2*, 815–826.

Beitel, G.J., and Krasnow, M.A. (2000). Genetic control of epithelial tube size in the Drosophila tracheal system. Development *127*, 3271–3282.

Bettoun, A., Joffre, C., Zago, G., Surdez, D., Vallerand, D., Gundogdu, R., Sharif, A.A., Gomez, M., Cascone, I., Meunier, B., et al. (2016). Mitochondrial clearance by the STK38 kinase supports oncogenic Ras-induced cell transformation. Oncotarget *7*, 44142–44160.

Boggiano, J.C., Vanderzalm, P.J., and Fehon, R.G. (2011). Tao-1 phosphorylates hippo/MST kinases to regulate the hippo-Salvador-warts tumor suppressor pathway. Dev. Cell *21*, 888–895.

Choi, H., Larsen, B., Lin, Z.Y., Breitkreutz, A., Mellacheruvu, D., Fermin, D., Qin, Z.S., Tyers, M., Gingras, A.C., and Nesvizhskii, A.I. (2011). SAINT: probabilistic scoring of affinity purification-mass spectrometry data. Nat. Methods *8*, 70–73.

Chung, H.L., Augustine, G.J., and Choi, K.W. (2016). Drosophila Schip1 links expanded and Tao-1 to regulate hippo signaling. Dev. Cell *36*, 511–524.

Cook, D., Hoa, L.Y., Gomez, V., Gomez, M., and Hergovich, A. (2014). Constitutively active NDR1-PIF kinase functions independent of MST1 and hMOB1 signalling. Cell Signal. *26*, 1657–1667.

Cornils, H., Kohler, R.S., Hergovich, A., and Hemmings, B.A. (2011). Human NDR kinases control G(1)/S cell cycle transition by directly regulating p21 stability. Mol. Cell. Biol. *31*, 1382–1395.

Dan, I., Watanabe, N.M., and Kusumi, A. (2001). The Ste20 group kinases as regulators of MAP kinase cascades. Trends Cell Biol. *11*, 220–230.

Deng, Y., Pang, A., and Wang, J.H. (2003). Regulation of mammalian STE20-like kinase 2 (MST2) by protein phosphorylation/dephosphorylation and proteolysis. J. Biol. Chem. *278*, 11760–11767.

Dietzl, G., Chen, D., Schnorrer, F., Su, K.C., Barinova, Y., Fellner, M., Gasser, B., Kinsey, K., Oppel, S., Scheiblauer, S., et al. (2007). A genome-wide transgenic RNAi library for conditional gene inactivation in Drosophila. Nature *448*, 151–156.

Draheim, K.M., Fisher, O.S., Boggon, T.J., and Calderwood, D.A. (2014). Cerebral cavernous malformation proteins at a glance. J. Cell Sci. *127*, 701–707.

Emoto, K., He, Y., Ye, B., Grueber, W.B., Adler, P.N., Jan, L.Y., and Jan, Y.N. (2004). Control of dendritic branching and tiling by the Tricornered-kinase/Furry signaling pathway in Drosophila sensory neurons. Cell *119*, 245–256.

Emoto, K., Parrish, J.Z., Jan, L.Y., and Jan, Y.N. (2006). The tumour suppressor Hippo acts with the NDR kinases in dendritic tiling and maintenance. Nature *443*, 210–213.

Förster, D., Armbruster, K., and Luschnig, S. (2010). Sec24-dependent secretion drives cell-autonomous expansion of tracheal tubes in Drosophila. Curr. Biol. *20*, 62–68.

Francis, D., and Ghabrial, A.S. (2015). Compensatory branching morphogenesis of stalk cells in the Drosophila trachea. Development *142*, 2048–2057.

Friedman, A., and Perrimon, N. (2006). A functional RNAi screen for regulators of receptor tyrosine kinase and ERK signalling. Nature *444*, 230–234.

Genevet, A., Polesello, C., Blight, K., Robertson, F., Collinson, L.M., Pichaud, F., and Tapon, N. (2009). The Hippo pathway regulates apical-domain size independently of its growth-control function. J. Cell Sci. *122*, 2360–2370.

Genevet, A., Wehr, M.C., Brain, R., Thompson, B.J., and Tapon, N. (2010). Kibra is a regulator of the Salvador/warts/Hippo signaling network. Dev. Cell *18*, 300–308.

Geng, W., He, B., Wang, M., and Adler, P.N. (2000). The tricornered gene, which is required for the integrity of epidermal cell extensions, encodes the Drosophila nuclear DBF2-related kinase. Genetics *156*, 1817–1828.

Ghabrial, A.S., Levi, B.P., and Krasnow, M.A. (2011). A systematic screen for tube morphogenesis and branching genes in the Drosophila tracheal system. PLoS Genet. *7*, e1002087.

Glantschnig, H., Rodan, G.A., and Reszka, A.A. (2002). Mapping of MST1 kinase sites of phosphorylation. Activation and autophosphorylation. J. Biol. Chem. *277*, 42987–42996.

Gomez, J.M., Wang, Y., and Riechmann, V. (2012). Tao controls epithelial morphogenesis by promoting Fasciclin 2 endocytosis. J. Cell Biol. *199*, 1131–1143.

Green, R.B., Hatini, V., Johansen, K.A., Liu, X.J., and Lengyel, J.A. (2002). Drumstick is a zinc finger protein that antagonizes Lines to control patterning and morphogenesis of the Drosophila hindgut. Development *129*, 3645–3656.

Halder, G., and Johnson, R.L. (2011). Hippo signaling: growth control and beyond. Development *138*, 9–22.

Harvey, K.F., Pfleger, C.M., and Hariharan, I.K. (2003). The Drosophila Mst ortholog, hippo, restricts growth and cell proliferation and promotes apoptosis. Cell *114*, 457–467.

Harvey, K.F., Zhang, X., and Thomas, D.M. (2013). The Hippo pathway and human cancer. Nat. Rev. Cancer *13*, 246–257.

Hergovich, A. (2013). Regulation and functions of mammalian LATS/NDR kinases: looking beyond canonical Hippo signalling. Cell Biosci *3*, 32.

Hergovich, A. (2016). The roles of NDR protein kinases in hippo signalling. Genes (Basel) *7*, 1–16.

Hergovich, A., Bichsel, S.J., and Hemmings, B.A. (2005). Human NDR kinases are rapidly activated by MOB proteins through recruitment to the plasma membrane and phosphorylation. Mol. Cell. Biol. *25*, 8259–8272.

Hergovich, A., and Hemmings, B.A. (2009). Mammalian NDR/LATS protein kinases in hippo tumor suppressor signaling. BioFactors *35*, 338–345.

Hergovich, A., and Hemmings, B.A. (2012). Hippo signalling in the G2/M cell cycle phase: lessons learned from the yeast MEN and SIN pathways. Semin. Cell Dev. Biol. *23*, 794–802.

Hergovich, A., Kohler, R.S., Schmitz, D., Vichalkovski, A., Cornils, H., and Hemmings, B.A. (2009). The MST1 and hMOB1 tumor suppressors control human centrosome duplication by regulating NDR kinase phosphorylation. Curr. Biol. *19*, 1692–1702.

Huang, J., Wu, S., Barrera, J., Matthews, K., and Pan, D. (2005). The Hippo signaling pathway coordinately regulates cell proliferation and apoptosis by inactivating Yorkie, the Drosophila homolog of YAP. Cell *122*, 421–434.

Huang, J., Zhou, W., Dong, W., and Hong, Y. (2009). Targeted engineering of the Drosophila genome. Fly (Austin) *3*, 274–277.

Huttlin, E.L., Ting, L., Bruckner, R.J., Gebreab, F., Gygi, M.P., Szpyt, J., Tam, S., Zarraga, G., Colby, G., Baltier, K., et al. (2015). The BioPlex network: a systematic exploration of the human interactome. Cell *162*, 425–440.

Jia, J., Zhang, W., Wang, B., Trinko, R., and Jiang, J. (2003). The Drosophila Ste20 family kinase dMST functions as a tumor suppressor by restricting cell proliferation and promoting apoptosis. Genes Dev. *17*, 2514–2519.

Jukam, D., Xie, B., Rister, J., Terrell, D., Charlton-Perkins, M., Pistillo, D., Gebelein, B., Desplan, C., and Cook, T. (2013). Opposite feedbacks in the Hippo pathway for growth control and neural fate. Science *342*, 1238016.

King, I., Tsai, L.T., Pflanz, R., Voigt, A., Lee, S., Jäckle, H., Lu, B., and Heberlein, U. (2011). Drosophila tao controls mushroom body development and ethanol-stimulated behavior through par-1. J. Neurosci. *31*, 1139–1148.

Kyriakakis, P., Tipping, M., Abed, L., and Veraksa, A. (2008). Tandem affinity purification in Drosophila: the advantages of the GS-TAP system. Fly (Austin) *2*, 229–235.

Lant, B., Yu, B., Goudreault, M., Holmyard, D., Knight, J.D., Xu, P., Zhao, L., Chin, K., Wallace, E., Zhen, M., et al. (2015). CCM-3/STRIPAK promotes seamless tube extension through endocytic recycling. Nat. Commun. *6*, 6449.

Lee, T., and Luo, L. (1999). Mosaic analysis with a repressible cell marker for studies of gene function in neuronal morphogenesis. Neuron *22*, 451–461.

Levi, B.P., Ghabrial, A.S., and Krasnow, M.A. (2006). Drosophila talin and integrin genes are required for maintenance of tracheal terminal branches and luminal organization. Development *133*, 2383–2393.

Li, Q., Li, S., Mana-Capelli, S., Roth Flach, R.J., Danai, L.V., Amcheslavsky, A., Nie, Y., Kaneko, S., Yao, X., Chen, X., et al. (2014). The conserved misshapen-warts-Yorkie pathway acts in enteroblasts to regulate intestinal stem cells in Drosophila. Dev. Cell *31*, 291–304.

Li, Q., Nirala, N.K., Nie, Y., Chen, H.J., Ostroff, G., Mao, J., Wang, Q., Xu, L., and Ip, Y.T. (2018). Ingestion of food particles regulates the mechanosensing misshapen-Yorkie pathway in Drosophila intestinal growth. Dev. Cell *45*, 433–449.e6.

Liu, T., Rohn, J.L., Picone, R., Kunda, P., and Baum, B. (2010). Tao-1 is a negative regulator of microtubule plus-end growth. J. Cell Sci. *123*, 2708–2716.

Lucas, E.P., Khanal, I., Gaspar, P., Fletcher, G.C., Polesello, C., Tapon, N., and Thompson, B.J. (2013). The Hippo pathway polarizes the actin cytoskeleton during collective migration of Drosophila border cells. J. Cell Biol. *201*, 875–885.

Meng, Z., Moroishi, T., Mottier-Pavie, V., Plouffe, S.W., Hansen, C.G., Hong, A.W., Park, H.W., Mo, J.S., Lu, W., Lu, S., et al. (2015). MAP4K family kinases act in parallel to MST1/2 to activate LATS1/2 in the Hippo pathway. Nat. Commun. *6*, 8357.

Myat, M.M., Lightfoot, H., Wang, P., and Andrew, D.J. (2005). A molecular link between FGF and Dpp signaling in branch-specific migration of the Drosophila trachea. Dev. Biol. *281*, 38–52.

Pan, D. (2010). The hippo signaling pathway in development and cancer. Dev. Cell *19*, 491–505.

Pantalacci, S., Tapon, N., and Léopold, P. (2003). The Salvador partner Hippo promotes apoptosis and cell-cycle exit in Drosophila. Nat. Cell Biol. *5*, 921–927.

Poon, C.L., Lin, J.I., Zhang, X., and Harvey, K.F. (2011). The Sterile 20-like kinase Tao-1 controls tissue growth by regulating the Salvador-Warts-Hippo pathway. Dev. Cell *21*, 896–906.

Poon, C.L., Mitchell, K.A., Kondo, S., Cheng, L.Y., and Harvey, K.F. (2016). The Hippo pathway regulates neuroblasts and brain size in Drosophila melanogaster. Curr. Biol. *26*, 1034–1042.

Poon, C.L., Zhang, X., Lin, J.I., Manning, S.A., and Harvey, K.F. (2012). Homeodomain-interacting protein kinase regulates hippo pathway-dependent tissue growth. Curr. Biol. *22*, 1587–1594.

Praskova, M., Xia, F., and Avruch, J. (2008). MOBKL1A/MOBKL1B phosphorylation by MST1 and MST2 inhibits cell proliferation. Curr. Biol. *18*, 311–321.

Ruiz, O.E., Nikolova, L.S., and Metzstein, M.M. (2012). Drosophila Zpr1 (zinc finger protein 1) is required downstream of both EGFR and FGFR signaling in tracheal subcellular lumen formation. PLoS One *7*, e45649.

Samakovlis, C., Hacohen, N., Manning, G., Sutherland, D.C., Guillemin, K., and Krasnow, M.A. (1996). Development of the Drosophila tracheal system occurs by a series of morphologically distinct but genetically coupled branching events. Development *122*, 1395–1407.

Shiga, Y., Tanaka-Matakatsu, M., and Hayashi, S. (1996). A nuclear GFP/β-galactosidase fusion protein as a marker for morphogenesis in living Drosophila. Dev. Growth Differ. *38*, 99–106.

Song, Y., Eng, M., and Ghabrial, A.S. (2013). Focal defects in single-celled tubes mutant for cerebral cavernous malformation 3, GCKIII, or NSF2. Dev. Cell *25*, 507–519.

Stegert, M.R., Hergovich, A., Tamaskovic, R., Bichsel, S.J., and Hemmings, B.A. (2005). Regulation of NDR protein kinase by hydrophobic motif phosphorylation mediated by the mammalian Ste20-like kinase MST3. Mol. Cell. Biol. *25*, 11019–11029.

Tamaskovic, R., Bichsel, S.J., Rogniaux, H., Stegert, M.R., and Hemmings, B.A. (2003). Mechanism of Ca2+-mediated regulation of NDR protein kinase through autophosphorylation and phosphorylation by an upstream kinase. J. Biol. Chem. *278*, 6710–6718.

Tapon, N., Harvey, K.F., Bell, D.W., Wahrer, D.C., Schiripo, T.A., Haber, D.A., and hariharan, I.K. (2002). Salvador promotes both cell cycle exit and apoptosis in Drosophila and is mutated in human cancer cell lines. Cell *110*, 467–478.

Udan, R.S., Kango-Singh, M., Nolo, R., Tao, C., and Halder, G. (2003). Hippo promotes proliferation arrest and apoptosis in the Salvador/Warts pathway. Nat. Cell Biol. *5*, 914–920.

Vissers, J.H., Manning, S.A., Kulkarni, A., and Harvey, K.F. (2016). A Drosophila RNAi library modulates Hippo pathway-dependent tissue growth. Nat. Commun. *7*, 10368.

Wu, S., Huang, J., Dong, J., and Pan, D. (2003). Hippo encodes a Ste-20 family protein kinase that restricts cell proliferation and promotes apoptosis in conjunction with Salvador and warts. Cell *114*, 445–456.

Yang, L., and Veraksa, A. (2017). Single-step affinity purification of ERK signaling complexes using the streptavidin-binding peptide (SBP) tag. Methods Mol. Biol. *1487*, 113–126.

Yoo, S.J., Huh, J.R., Muro, I., Yu, H., Wang, L., Wang, S.L., Feldman, R.M., Clem, R.J., Müller, H.A., and Hay, B.A. (2002). Hid, Rpr and Grim negatively regulate DIAP1 levels through distinct mechanisms. Nat. Cell Biol. *4*, 416–424.

Yoruk, B., Gillers, B.S., Chi, N.C., and Scott, I.C. (2012). Ccm3 functions in a manner distinct from Ccm1 and Ccm2 in a zebrafish model of CCM vascular disease. Dev. Biol. *362*, 121–131.

Yu, F.X., and Guan, K.L. (2013). The Hippo pathway: regulators and regulations. Genes Dev. *27*, 355–371.

Yu, J.A., Castranova, D., Pham, V.N., and Weinstein, B.M. (2015). Single-cell analysis of endothelial morphogenesis in vivo. Development *142*, 2951–2961.

Zalvide, J., Fidalgo, M., Fraile, M., Guerrero, A., Iglesias, C., Floridia, E., and Pombo, C.M. (2013). The CCM3-GCKIII partnership. Histol. Histopathol. *28*, 1265–1272.

Zheng, Y., Wang, W., Liu, B., Deng, H., Uster, E., and Pan, D. (2015). Identification of Happyhour/MAP4K as alternative Hpo/Mst-like kinases in the hippo kinase cascade. Dev. Cell *34*, 642–655.

STAR★METHODS

KEY RESOURCES TABLE

REAGENT or RESOURCE	SOURCE	IDENTIFIER
Antibodies		
Mouse monoclonal anti-DIAP1	Yoo et al. (2002)	N/A
Rabbit anti-Varicose	Bachmann et al. (2008)	N/A
Mouse anti-Coracle (a cocktail of C566.9C and C615.16A, each at1:500)	Developmental Studies Hybridoma Bank	Cat# C566.9; RRID:AB_1161642 & C615.16; RRID: AB_1161644
Mouse anti-Fasciclin 3	Developmental Studies Hybridoma Bank	Cat# 7G10 anti-Fasciclin III; RRID:AB_528238
Rabbit polyclonal anti-phospho-NDR1-Thr444	Tamaskovic et al. (2003)	N/A
Rabbit anti-cleaved Drosophila Dcp1 (Asp216)	Cell Signaling Technology	Cat# 9578; RRID:AB_2721060
Chicken polyclonal anti-GFP	Abcam	Cat# ab13970; RRID:AB_300798
Rabbit monoclonal anti-HA (C29F4)	Cell Signaling Technology	Cat# 3724; RRID:AB_1549585
Rat monoclonal anti-HA (3F10)	Roche	Cat# 11867423001; RRID:AB_10094468
Mouse monoclonal anti-myc (9E10)	Santa Cruz Biotechnology	Cat# sc-40; RRID:AB_627268
Rabbit monoclonal anti-myc (71D10)	Cell Signaling Technology	Cat# 2278; RRID: AB_10693332
Mouse monoclonal anti-MST3	BD Biosciences	Cat# 611057; RRID: AB_398370
Rabbit polyclonal anti-MST4	Cell Signaling Technology	Cat# 3822S; RRID: AB_10694686
Goat polyclonal anti-STK25	Santa Cruz Biotechnology	Cat# sc-6865; RRID: AB_2198792
Goat polyclonal anti-actin	Santa Cruz Biotechnology	Cat# sc-1616; RRID: AB_630836
Mouse monoclonal anti-Mal (Maltose binding protein)	New England BioLabs	Cat# E8032; RRID:AB_1559730
Rabbit monoclonal anti-MST4 + MST3 + STK25 (phospho T178 + T190 + T174) antibody [EP2123Y]	Abcam	Cat# ab76579; RRID: AB_1523983
Goat anti-chicken 488	Thermo Fisher Scientific	Cat#A11039; RRID:AB_142924
Donkey anti-mouse 555	Thermo Fisher Scientific	Cat#A31570; RRID:AB_2536180
Sheep anti-Mouse IgG - Horseradish peroxidase linked antibody	GE Healthcare	Cat#NA931; RRID: AB_772210
Donkey anti-Rabbit IgG Horseradish peroxidase linked antibody	GE Healthcare	Cat#NA934; RRID: AB_2722659
Goat anti-Rat IgG Horseradish peroxidase linked antibody	GE Healthcare	Cat#NA935; RRID: AB_772207
Chemicals, Peptides, and Recombinant Proteins		
GST-MST1 (M9697)	Carna Biosciences	Cat# 07-116
GST-MST2 (S6573)	Carna Biosciences	Cat# 07-117
GST-MST3 (M9822)	Carna Biosciences	Cat# 07-118
GST-MST4 (M9947)	Carna Biosciences	Cat# 07-119
GST-STK25 (SRP5087)	Carna Biosciences	Cat# 07-136
Dulbecco's Modified Eagle's Medium (DMEM)	Sigma	Cat# D6429
Fetal bovine serum (FBS)	Sigma	Cat# F7524
Fugene 6	Promega	Cat# E2692
Schneider's Medium	Thermo Fisher Scientific	Cat# 217200024
Heat inactivated fetal bovine serum	Thermo Fisher Scientific	Cat# 10082147
Effectene	Qiagen	Cat# 301425
Amylose resin	New England Biolabs	Cat# E8021
Critical Commercial Assays		
Click-iT® EdU Alexa Fluor® 555 Imaging Kit	Thermo Fisher	Cat# C10338

(*Continued on next page*)

Continued

REAGENT or RESOURCE	SOURCE	IDENTIFIER
Experimental Models: Cell Lines		
Human: HEK293 cells	ATCC	Cat# CRL-1573
D. melanogaster: Cell line S2R+	Drosophila Genomics Resource Center	Cat# 150
D. melanogaster: Stable cell line S2 expressing pMK33-NTAP-GS-Tao-1	This study	N/A
Experimental Models: Organisms/Strains		
D.melanogaster: w; Tao^{eta} FRT19A	Gomez et al. (2012)	N/A
D.melanogaster: w; FRT82B GckIII^{wheezy770}	Song et al. (2013)	N/A
D.melanogaster: w; FRT42D hpo$^{5.1}$	Genevet et al. (2009)	N/A
D.melanogaster: w; FRT42D hpo$^{42-47}$	Wu et al. (2003)	N/A
D.melanogaster: w; trc^{1} FRT80B	Geng et al. (2000)	N/A
D.melanogaster: y w eyFLP; FRT82B P[mini-w, ubi-GFP]	This study	N/A
D.melanogaster: y w eyFLP, UAS-GFP; tub-GAL4, FRT42D, tub-GAL80	This study	N/A
D.melanogaster: y w hsFLP, UAS-GFP; tub-GAL4, FRT42D, tub-GAL80	This study	N/A
D.melanogaster: yw hsFLP^{122}; FRT42D tub-GAL80; btl-Gal4, UAS-GFP	Francis and Ghabrial (2015)	N/A
D.melanogaster: yw hsFLP^{122}; btl-Gal4, UAS-GFP; FRT80B tub-Gal80	This study	N/A
D.melanogaster: UAS-GFP RNAi, hsFLP^{122}, FRT19A; btl-Gal4, UAS-GFP, UAS-DsREDnls	Levi et al. (2006)	N/A
D.melanogaster: y w hsFLP^{122}; btl-GAL4, UAS-DsREDnls; FRT82B cu UASi-GFPhp/TM6B	Ghabrial et al. (2011)	N/A
D.melanogaster: hh-Gal4	Genevet et al. (2010)	N/A
D.melanogaster: rn-Gal4	Bloomington Drosophila Stock Center	BDSC: 7405
D.melanogaster: btl-Gal4	Shiga et al. (1996)	BDSC: 8807
D.melanogaster: drm-Gal4	Green et al. (2002)	N/A
D.melanogaster: UAS-Tao-1 RNAi GD	Vienna Drosophila Resource Center	17432
D.melanogaster: UAS-Tao-1 RNAi.8 (modified VDRC KK 107645 that has a *P* element-containing insertion removed from the *40D* locus by meiotic recombination)	Vissers et al. (2016)	107645.8
D.melanogaster: UAS-GckIII RNAi	Vienna Drosophila Resource Center	107158
D.melanogaster: UAS-trc RNAi	Vienna Drosophila Resource Center	107923
D.melanogaster: crumbs-GFPA	Huang et al. (2009)	N/A
D.melanogaster: UAS-Tao-1^{HA}: UAS-Tao-1Δ423-900	This study	N/A
D.melanogaster: UAS-GckIII^{HA}: UAS-GckIII^{T167D}	This study	N/A
D.melanogaster: UAS-GckIII^{DN}: UAS-GckIII ^{T167A}	This study	N/A
Recombinant DNA		
pAW vector	Drosophila Genomics Resource Center	1127
pcDNA3_HA	Hergovich et al. (2005)	N/A
pcDNA3_myc	Bettoun et al. (2016)	N/A
pENTR-3C	Invitrogen	Cat# A10464
pMK33-NTAP-GS-Tao-1	This study	N/A

(*Continued on next page*)

Continued

REAGENT or RESOURCE	SOURCE	IDENTIFIER
pAW_HA-Tao1	This study	N/A
pcDNA3_HA-Tao-1	This study	N/A
pcDNA3_HA-Tao-1-D168A	This study	N/A
pcDNA5-TAO1	Poon et al. (2011)	N/A
pcDNA5-TAO1-K57A	Poon et al. (2011)	N/A
pcDNA3-HA-TAO1	This study	N/A
pcDNA3-HA-TAO1-K57A	This study	N/A
pcDNA3_myc-TAO1	This study	N/A
GckIII cDNA	Drosophila Genomics Resource Center	RE38276
pcDNA3_myc-GckIII	This study	N/A
pcDNA3_myc-GckIII-K42R	This study	N/A
pcDNA3_HA-MST3	This study	N/A
pcDNA3_HA-MST4	This study	N/A
pcDNA3_HA-STK25	This study	N/A
pMal-c2-GckIII	This study	N/A
pMal-c2-GckIII-K42R	This study	N/A
pMal-c2-GckIII-T167A	This study	N/A
pMal-c2-MST3 (kinase-dead)	This study	N/A
pMal-c2-MST4 (kinase-dead)	This study	N/A
pMal-c2-STK25 (kinase-dead)	This study	N/A
pMal-Trc(HM)	This study	N/A
pMal-NDR1(HM)	This study	N/A
pMal-NDR2(HM)	This study	N/A
pcDNA3_HA-TAO1	This study	N/A
Software and Algorithms		
SAINT software	Choi et al. (2011)	N/A
Adobe Photoshop	Adobe	RRID:SCR_014199
GraphPad Prism	GraphPad Software	RRID:SCR_002798

CONTACT FOR REAGENT AND RESOURCE SHARING

Further information and requests for resources and reagents should be directed to and will be fulfilled by the Lead Contact, Kieran F. Harvey (kieran.harvey@petermac.org).

EXPERIMENTAL MODEL AND SUBJECT DETAILS

Drosophila melanogaster stocks were maintained on standard medium at room temperature (22°C) and experimental crosses were carried out at 25°C, unless otherwise indicated.

D. melanogaster S2R+ and S2 cells were maintained at 24°C in Schneider's Medium (217200024, Invitrogen) supplemented with heat inactivated FBS (10082147, Invitrogen) and penicillin/streptomycin.

HEK293 cells were grown at 37°C in 5% CO2 humidified chambers in DMEM (D6429, Sigma) supplemented with 10% fetal bovine serum (FBS; F7524, Sigma) and penicillin/streptomycin.

METHOD DETAILS

D. melanogaster Stocks

w; Tao^{eta} FRT19A (Veit Riechmann)
w; FRT82B GckIII^{wheezy770}
w; FRT42D hpo$^{5.1}$ (Nic Tapon)
w; FRT42D hpo$^{42-47}$
w; trc^{1} FRT80B (Paul Adler)

y w eyFLP; FRT82B P[mini-w, ubi-GFP]
y w eyFlp, UAS-GFP; tub-GAL4, FRT42D, tub-GAL80
yw hsFLP^{122}; FRT42D tub-GAL80; btl-Gal4, UAS-GFP
yw hsFLP^{122}; btl-Gal4, UAS-GFP; FRT80B tub-Gal80
ywhsFLP^{122}; FRT42D tub-Gal80; FRT82B GFPi
UAS-GFP RNAi, hsFLP^{122}, FRT19A; btl-Gal4, UAS-GFP, UAS-DsREDnls
y w hsFLP^{122}; btl-GAL4, UAS-DsREDnls; FRT82B cu UASi-GFPhp/TM6B
GAL4 lines: *hh-GAL4*, *btl-GAL4*, *drm-GAL4* and *rn-Gal4* (Bloomington Drosophila Stock Center).

UAS-RNAi lines: *UAS-Tao-1 RNAi* (VDRC GD 17432), *UAS-Tao-1 RNAi* (107645.8, modified VDRC KK 107645 that has a P element-containing insertion removed from the 40D locus by meiotic recombination (Vissers et al., 2016), *UAS-Trc RNAi* (VDRC KK 107923), *UAS-GckIII RNAi* (VDRC KK 107158), all Vienna Drosophila RNAi Center (Dietzl et al., 2007).

Other stocks: *crumbs-GFPA* (Yang Hong).

Transgenic flies: *UAS-Tao-1^{HA}* is a dominant active form of Tao-1 that contains a deletion of residues 423-900 (Liu et al., 2010). *UAS-Tao-1^{HA}* flies were generated by subcloning V5-epitope tagged *Tao-1Δ423-900* cDNA into *pUAST*. The *pUAST-Tao-1Δ423-900* DNA sequence was confirmed by Sanger sequencing and transgenic flies created by BestGene Inc. To generate *UAS-GckIII^{HA}*, the wild type *GckIII* cDNA was subjected to site directed mutagenesis (Quickchange, Agilent) to introduce a T to D coding change at amino acid residue 167. The cDNA was cloned into the *pUAST* vector, injected into embryos (Rainbow Transgenic Flies) and transgenic lines established. To generate an HA-epitope tagged *UAS-GckIII^{DN}*, *HA-GckIII^{T167A}* cDNA was generated by PCR mutagenesis, cloned into the *pTW* vector via Gateway cloning (Thermo Fisher Scientific), confirmed by Sanger sequencing and transgenic flies created by BestGene Inc.

Generation of Clones in *Drosophila*

For analysis of mosaic wing imaginal discs, clones were generated by heat shock on day 2 for 10 minutes at 37°C, incubating crosses at 25°C and wing discs were dissected from mosaic larvae on day 5. For analysis of mosaic trachea cells in larvae, clones were generated by heat shocking 0-4 hr old embryos for 1 hour at 38°C, incubating crosses at 25°C for 5 days and selecting third instar mosaic larvae for analysis. Larvae were heat killed or filleted as described previously (Ghabrial et al., 2011).

Immunofluorescence

Primary antibodies were specific for DIAP1 (B. Hay), Varicose (E. Knust), Coracle, Fasciclin 3 (both DSHB), p-Thr444P (NDR1) (Tamaskovic et al., 2003), cleaved Dcp1 (Cell Signalling) and anti-GFP (Abcam). Anti-rat, anti-Chicken and anti-mouse secondary antibodies were from Invitrogen. Tissues were fixed and stained as in (Poon et al., 2012; Song et al., 2013).

Cell Proliferation Assay

EdU (5-ethynyl-2'deoxyuridine) incorporation assays were used to assess cell proliferation as in (Poon et al., 2016). Third instar eye imaginal discs were dissected and subjected to 1 hour incubation with 10μM EdU/PBS, then fixed for 20 minutes in 4% formaldehyde/PBS. Incorporated EdU was detected by Click-iT fluorescent dye azide reaction in accordance to manufacturer's instructions (Life technologies).

Transient Transfections of Cultured Cells

Exponentially growing HEK293 cells were plated at a consistent confluence and transfected with plasmids using Fugene 6 (E2692, Promega) according to the manufacturer's instructions.

S2R+ cells were transiently transfected with pAW-based plasmids using Effectene (301425, Qiagen) according to the manufacturer's instructions.

Expression Plasmids

The *D. melanogaster* Tao-1 open reading frame was cloned into the pMK33-NTAP-GS vector (Kyriakakis et al., 2008), to generate N-terminally tagged Tao-1. *D. melanogaster* Tao-1 and human TAO1, MST3, MST4 and STK25 cDNAs were described (Hergovich et al., 2009; Poon et al., 2011). The pAW vector and *D. melanogaster* GckIII cDNA (RE38276) were from the *Drosophila* Genomics Resource Center (Indiana University, USA). pcDNA3_HA and pcDNA3_myc vectors were reported (Hergovich et al., 2005; Bettoun et al., 2016). To generate N-terminally tagged cDNAs, human TAO1 was subcloned with *BamH*I and *EcoR*I into modified pcDNA3_HA or pcDNA3_myc. *D. melanogaster* Tao-1 and GckIII were subcloned with *BamH*I and *Xho*I into modified pcDNA3_HA or pcDNA_myc, respectively. *D. melanogaster* GckIII kinase-dead (K42R) or activation loop phospho-acceptor (T167A) mutants were generated by PCR mutagenesis using wild-type GckIII as a template. To subclone N-terminally tagged cDNAs into the pAW *D. melanogaster* expression vector, tagged cDNAs were first inserted into the pENTR-3C plasmid (Invitrogen) and then recombined into the pAW destination plasmid using Gateway technology (Invitrogen). All constructs were confirmed by Sanger sequencing.

Immunoblotting, Immunoprecipitations, and Antibodies

Immunoblotting and co-immunoprecipitation experiments were performed as described (Hergovich et al., 2005). The characterization of Tao-1 and TAO1 binding to GCKIII kinases was carried out in low-stringency buffer as defined previously (Cook et al., 2014).

Anti-HA antibodies were from Cell Signaling (C29F4) and Roche (3F10). Anti-myc antibodies were from Santa Cruz Technology (9E10) and Cell Signaling Technology (71D10). Anti-MST3 (611057) was from BD Biosciences, anti-MST4 (3822) was from Cell Signaling Technology, anti-STK25 (sc-6865) and anti-actin (sc-1616) were from Santa Cruz Biotechnology. anti-Mal (Maltose binding protein; E8032) is from New England BioLabs. The antibody detecting activation loop phosphorylation of GckIII (Thr167), MST3 (Thr190), MST4 (Thr178) and STK25 (Thr174) was from Abcam and termed anti-T167-P or anti-GCKIII-P, respectively. The antibody detecting hydrophobic motif phosphorylation of Trc (Thr449) has been described (Tamaskovic et al., 2003). Secondary antibodies were purchased from GE Healthcare (NA931, NA934, and NA935) and Santa Cruz Biotechnology (sc-2020).

Mass Spectrometry

pMK33-NTAP-GS-Tao-1 was transfected into *D. melanogaster* S2 cells and a stable cell line was selected using hygromycin. Protein complexes containing Tao-1 and associated interactors were purified as in (Yang and Veraksa, 2017) and analysed by nanoLC-MS/MS. Results from two independent biological replicates were compared to six independent controls using SAINT software (Choi et al., 2011).

Kinase Assays

Full-length *D. melanogaster* GckIII and human MST3, MST4 or STK25 cDNAs were inserted into the pMal-c2 vector (New England BioLabs) using *BamH*I and *Xho*I/*Sal*I or *Xba*I sites to generate pMal-GckIII/GCKIII plasmids, which can express kinase-dead versions that are N-terminally tagged by the maltose binding protein (Mal). The C-terminal hydrophobic fragments of *D. melanogaster* Trc (residues 308 to 459), human NDR1 (residues 301 to 465) and NDR2 (residues 302 to 464) were inserted into the pMal-c2 vector using *BamH*I and *Xho*I/*Sal*I sites to generate pMal-Trc/NDR(HM) plasmids. Recombinant Mal-fusion proteins were expressed in *E. coli* BL21(DE3) at 30°C and purified using amylose resin (E8021, New England BioLabs) as described (Hergovich et al., 2005). Recombinant full-length GST-MST1 (M9697; 07-116), GST-MST2 (S6573; 07-117), GST-MST3 (M9822; 07-118), GST-MST4 (M9947; 07-119) and GST-STK25 (SRP5087; 07-136) were from Sigma and Carna Biosciences, respectively. To produce immunopurified full-length HA-tagged Tao-1 or TAO1 kinase version, *D. melanogaster* S2R+ or human HEK293 cells were transfected with pAW_HA-Tao1 or pcDNA3_HA-TAO1 and processed for immunoprecipitation (IP) using anti-HA antibody and stringent IP conditions as described (Hergovich et al., 2005). Immunopurified proteins were washed twice with kinase buffer (50 mM Hepes pH 7.4, 10 mM $MgCl_2$, 2.5 mM beta-glycerophosphate, 1 mM EGTA, 1 mM Na_3VO_4, 1 mM NaF, 0.01 mM DTT), before kinase reactions were performed as follows: per reaction, 200 ng of Mal-fusion proteins were incubated at 30°C for 30 minutes in 20 μl of kinase buffer containing 100 μM ATP in the absence or presence of immunopurified Tao-1, TAO1 or GCKIII or GST-tagged kinases (100 ng per reaction). Reactions were stopped by the addition of Laemmli buffer, separated by SDS-PAGE, and immunoblotted as outlined above.

QUANTIFICATION AND STATISTICAL ANALYSIS

In Figures S1E and S1J, control and experimental samples were analysed in one experiment. Adult posterior wing area and imaginal disc clones were measured using Adobe Photoshop software (Adobe), and statistical analyses and graphs were plotted using Graph Pad Prism (GraphPad software). Error bars represent standard error of mean (s.e.m.) and unpaired t-tests were used to assess statistical differences, assuming Gaussian distribution and using two-tailed P value. n values are stated in legends. In Figure S1E, the t-value (t) was 10.5 and the degree of freedom (df) was 25. In Figure S1J, the t and df values, respectively, are: control vs *GckIII Ri*: t=1.76 df=8; control vs $hpo^{5.1}$: t=6.469 df=7; $hpo^{5.1}$ vs $hpo^{5.1}$+ *GckIII Ri*: t=0.3452 df=6.

In Figures 1A, 1C, 1D, 2, 6B, and 6C, Western blots and kinase assays were repeated at least three times. In each experiment, no statistical method was used to predetermine sample size, the experiments were not randomized and the investigators were not blinded to allocation during experiments or outcome assessment.